JOURNAL OF GEOPHYSICAL RESEARCH, VOL. ???, XXXX, DOI:10.1029/,

Determining North Atlantic meridional transport variability from pressure on the western boundary: A model investigation

R. J. Bingham

Proudman Oceanographic Laboratory, 6 Brownlow St., Liverpool, U.K.

C. W. Hughes

Proudman Oceanographic Laboratory, 6 Brownlow St., Liverpool, U.K.

R. J. BINGHAM, Proudman Oceanographic Laboratory, 6 Brownlow St., Liverpool, U.K. (rjbi@pol.ac.uk)

Abstract. In this paper we investigate the possibility of determining North Atlantic meridional transport variability using pressure on the western boundary, focusing on the 42°N latitude of the Halifax WAVE array. We start by reviewing the theoretical foundations of this approach. Next we present results from a model analysis, both statistical and dynamic, that demonstrate the feasibility of the approach. We consider how well we can quantify the meridional transport variability at 42°N given complete knowledge of bottom pressure across the basin, and to what degree this quantification is degraded by first ignoring the effect of intervening topography, and then by using only bottom pressure on the western boundary. We find that for periods of greater than one year we can recover more than 90% of the variability of the main overturning cell at 42°N using only the western boundary pressure, provided we remove the depth-average boundary pressure signal. This signal arises from a basin mode of bottom pressure variability, which has power at all timescales, but that does not in truth have a meridional transport signal associated with it, and from the geostrophic depth-independent compensation of the Ekman transport. An additional benefit of the removal of the depth-average pressure is that this high-frequency Ekman signal, which is essentially noise as far as monitoring the MOC for climatically important changes is concerned, is clearly separated from other modes.

1. Introduction

The North Atlantic meridional overturning circulation (MOC) characterises the process whereby relatively warm water in the upper 1000m or so of the ocean is transported to high latitudes, where upon it has cooled sufficiently to sink and return towards the equator in a cold deep layer. Because the MOC redistributes poleward a significant fraction of the solar energy received at the equator it is believed that the collapse of the MOC could have dramatic consequences for northern hemisphere climate, particularly for Northwest Europe [*Vellinga and Wood*, 2002; *Wood et al.*, 2003]. Even a more gradual slow down, as predicted by most climate models [*Cubasch et al.*, 2001] would have a significant impact on regional patterns of climate change. For this reason, a large effort is presently underway to monitor the Atlantic MOC.

A comprehensive monitoring array, deployed in 2004, spans almost the entire Atlantic basin at 26°N, with the objective of providing a daily estimate of the strength of the Atlantic MOC. The design of the array is described by *Hirschi et al.* [2003]. There are good reasons to focus on 26°N. Conveniently, at this latitude the Gulf Stream, which makes up the bulk of the northward transport, flows through the relatively shallow (≈800m) Florida Straits, where it can be monitored using voltage across an existing under-sea cable. It is believed that 26°N is near the latitude of maximum meridional heat transport, the quantity that is perhaps most directly related to climate variability. Also, 26°N is close to a traditional hydrographic section, therefore hydrographic observations at this latitude span a number of decades, allowing the variability observed by the array to be set in the context of an existing record, as has already been done by *Bryden et al.* [2005].

Since its deployment the array has produced a near continuous record of the meridional transport at 26°N. The results from the first year of observations have recently been published by *Cunningham et al.* [2007] and *Kanzow et al.* [2007]. The closure of the various individually measured components of the transport budget as demonstrated by *Kanzow et al.* [2007] validates the ability of the array to determine the transport variability. However, the large intra-annual variability of several Sv at all depths as reported by *Cunningham et al.* [2007] means that slowdowns or trends such as those claimed by *Bryden et al.* [2005] are difficult to detect over the short term.

Modelling studies by a number of authors have suggested that changes in the rate of deep water formation at high latitudes, as would be associated with a collapse or slowdown of the MOC, are communicated to lower latitudes by rapidly propagating coastally trapped waves [e.g. *Kawase*, 1987; *Johnson and Marshall*, 2002]. These waves leave in their wake a modified flow to ensure that the supply of water to high latitudes balances the rate of deep water production. This suggests that even on short timescales MOC variations should be meridionally coherent. However, recently *Bingham et al.* [2007] have shown that interannual variability of the meridional transport zonally integrated across the basin at one latitude may not be representative of the variability at other latitudes. (Henceforth we use meridional transport as shorthand for the meridional volume transport zonally integrated across the basin.)

Since it is not economically viable to repeat the comprehensive 26°N effort at a number of other latitudes to determine the true meridional coherence of the North Atlantic meridional transport, a less costly alternative is desirable. Fortunately, there are theoretical reasons to believe that the strongest manifestation of meridional transport variability

occurs on the western boundary. This raises the question of whether the meridional transport variability could be adequately monitored with an array situated only on the western boundary.

As a first step towards this, we consider, using an eddy permitting ocean model, to what extent variations in the Atlantic meridional transport at 42°N can be determined using only pressure on the western boundary. This particular latitude was chosen since it is the latitude of an existing observational campaign by the Proudman Oceanographic Laboratory, although not one currently designed to determine meridional transport variability in the sense described in this paper. We find, in the context of the model, where full knowledge of the western boundary pressure is available, that interannual variations of the meridional transport are reliably determined using only pressure on the western boundary. Moreover, for reasons described below, the array is, by design, insensitive to high-frequency variations of the meridional transport, and so acts as a low-pass filter eliminating the irrelevant short-lived fluctuations of the meridional transport.

In the next section we establish the theoretical basis for the relationship between bottom pressure on the western boundary and MOC variability. Then in section 3 we focus on 42°N where our present array is located. We examine the nature of bottom pressure, sea-surface height (SSH) and meridional transport variability at this latitude in an ocean model OCCAM, paying particular attention to the western boundary. Having established in a qualitative fashion the clear relationship between western boundary bottom pressure and the meridional transport, in section 4 we examine the relationship in terms of geostrophic balance and show quantitatively that measurements on the western boundary are indeed sufficient to estimate the interannual variability of the meridional transport to

a high degree of accuracy. Finally, in section 5 we discuss the implications of our results and draw some conclusions on monitoring the MOC.

2. Theoretical Basis

The theory behind monitoring meridional transport using boundary pressure is at first sight quite straightforward. It is based on the dominance of geostrophic balance for large-scale flows, and results from a zonal integral of the zonal momentum equation:

$$\int_W^E \rho_0 u_t - \rho_0 f v \, dx = \int_W^E (-p_x + \tau_z^x) \, dx, \tag{1}$$

where $x = r\lambda \cos\phi$, for latitude ϕ, longitude λ, and distance r from the centre of the earth. Here, the integral is at constant depth z from the western boundary $x = W(\phi, z)$ to the east $x = E(\phi, z)$. Nonlinear momentum terms have been neglected, as has lateral friction, but vertical friction is included as the vertical derivative of the zonal stress τ^x.

The acceleration term can be expected to be small on timescales much longer than a day; this is confirmed by angular momentum diagnostics [*Ponte and Rosen*, 1994]. In addition, below the surface Ekman layer, the stress term should be small (it may be significant in a bottom boundary layer, but such a layer will only occupy a small part of the zonal integral at a particular depth). Writing the zonal integral of v as T, and neglecting acceleration and stress terms reduces (1) to

$$\rho_0 f T = p_E - p_W, \tag{2}$$

i.e. the northward transport integrated along a particular depth and latitude line is simply given by the pressure difference between the end points of the line, divided by the Coriolis parameter f and reference density ρ_0. Throughout we shall refer to p_E and p_W as the eastern and western boundary pressures, respectively. By this we mean that they are the

bottom pressure (anomalies) at the eastern-most and western-most points of the ocean floor at a given depth (and latitude). It follows that $p_E(z)$ and $p_W(z)$ are defined for all $z \leq -H$, where H is the greatest depth of the ocean at the given latitude. This may mean that in the real ocean either one of $p_E(z)$ or $p_W(z)$ may be defined well outside what is conventional considered to be the boundary region.

It may seem overly simplistic to use this equation in the real ocean, where the zonal integral involves passing through a western boundary current in which nonlinear terms and perhaps other ageostrophic terms are important. However, while ageostrophic terms may be significant in the along-stream momentum balance of a boundary current, theoretical investigations generally accept that the cross-stream balance is dominated by geostrophy. Along-steam terms enter the zonal integral when the current is not meridional, but only weakly as long as they result from a narrow current, as in this case. Similarly, while eddies may be responsible for significant mass fluxes within density layers of varying thickness, the role of the associated ageostrophic flow in producing transport between two fixed, constant depth surfaces is much smaller. There is good reason to hope that geostrophy will work well in this integral balance.

Supporting evidence for this concept is found in *Hughes and de Cuevas* [2001], who showed that there is a rather good balance between wind stress and form stress in zonal integrals at all latitudes within the OCCAM model, confirming similar diagnostics based on the Southern Ocean in other models [*Stevens and Ivchenko*, 1997; *Gille*, 1997]. Form stress is defined as the zonal integral

$$-\int_W^E p_b H_x \, dx, \tag{3}$$

where p_b is bottom pressure and H is ocean depth (with this sign, it represents the eastward force exerted on the topography by the ocean). Performing the integral along the seafloor, we can write $H_x = -z_x$, so that the form stress becomes

$$-\int_W^E p_b H_x \, dx = \int_W^E p_b \, dz, \tag{4}$$

where dz is negative on the western side of an ocean basin, as depth increases eastwards, and positive on the eastern side as depth decreases. Alternatively, limiting the integral to a single ocean basin, this can be written as

$$-\int_W^E p_b H_x \, dx = \int_{-H_0}^0 (p_E - p_W) \, dz. \tag{5}$$

Comparing with (2), we see that the form stress is simply the depth-integrated northward geostrophic transport, divided by $\rho_0 f$. A balance between wind stress and form stress in a zonal integral then represents a balance between the northward Ekman flux across a particular latitude, and a geostrophic return flow. In Fig. 3 of *Hughes and de Cuevas* [2001], this balance is accurate to better than 50,000 Nm^{-1}, equivalent to about 0.5 Sv in transport, for latitudes of 40–50°N (integrated across both Atlantic and Pacific oceans), so we may expect this order of accuracy in depth-integrated transports calculated from (2), excluding the Ekman contribution.

However, in this study we are interested not in the balance between Ekman flow and return flow, but between a shallow and a deep limb of an overturning cell. The calculations presented in Section 4 address the accuracy of this balance within OCCAM. It is worthwhile first to point out some subtleties in this diagnostic.

The domain of integration is sketched schematically in Figure 1, on which we note the expected directions of zonal integral flow above the Mid-Atlantic Ridge. According to (2)

pressure on the western boundary is lower than at corresponding depths on the east for depths where the flow is northwards, and higher where the flow is southwards. Clearly, for the time mean flow, we need to know pressure both at the east and at the west. However, for variations in the flow, it is not at first obvious whether the associated pressure signal will be at the west or at the east, or a combination of the two. In fact, we expect changes in pressure to be stronger at the west than at the east, for the same reason that boundary currents are stronger on the west than the east.

This is a feature of simplified models such as *Kawase* [1987] and *Johnson and Marshall* [2002], in which changes in overturning are mediated by boundary waves which allow a trapped pressure signal at the western boundary to balance the flow in the boundary current, but which radiate into the interior from the eastern boundary leaving only small pressure signals at the east. More generically, the link between pressure signals and boundary currents is demonstrated by *Hughes and de Cuevas* [2001], who show that the primary large-scale balance in western boundary currents is $\rho_0 \beta V = J(p_b, H)$, where V is the depth-integrated northward flow and $\beta = df/dy$ ($y = r\phi$). The Jacobian term is a measure of the gradient of pressure along depth contours. In fact, integrating over a thin strip A bounded by two depth contours $z = -H_1$ (deeper) and $z = -H_2$ (shallower), and by two nearby latitudes separated by a meridional distance δy leads to

$$\frac{1}{\delta y} \int_A J(p_b, H)\, dA = \oint p_b \nabla H \cdot \mathbf{ds} = \frac{d}{dy} \int_{-H_1}^{-H_2} p_b\, dz, \tag{6}$$

which, comparing with (2), is the meridional derivative of the contribution of pressure at this boundary to f times the zonal integral of northward transport, integrated over the depth range $z = -H_1$ to $z = -H_2$ (p_b being the same as p_W on the western continental slope).

In other words, the bottom pressure variations associated with the zonally-integrated flow T in (2) are also associated with a depth-integrated flow V above the slope, via the bottom pressure torque. If variations in depth-integrated flow are much larger at the western boundary than the east, then we should expect the corresponding pressure changes to be at the western boundary rather than the east.

There is, however, a potential problem with assuming that eastern boundary pressure is constant. This results from the possibility of modes of variability in pressure which do not produce changes in either zonally-integrated northward flow, or in depth-integrated flow. This is true of any change of the form $p_b(H)$ in which the bottom pressure change is a function of depth only.

One such mode is well-known: at a period of about 5 days, changes in atmospheric pressure loading of the Atlantic and Pacific occur, but there is insufficient time for mass exchange between the ocean basins for the ocean to respond in an inverse barometer manner to these changes, although mass redistribution within each basin can occur. As a result, there are almost uniform basinwide signals in bottom pressure at this period [*Ponte*, 1997; *Mathers and Woodworth*, 2004; *Park and Watts*, 2006; *Stepanov and Hughes*, 2006]. Similarly, if for any reason the total ocean mass in the Atlantic were to change at longer periods, without any local change in wind stress or density forcing, we would expect a barotropic adjustment process to quickly distribute this mass uniformly over the area of the ocean, resulting in a uniform bottom pressure change.

Changes like this would result in changes in pressure on the western boundary which would be interpreted using (2) as a net northward flow at all depths, although such a flow does not in fact occur because there is a compensating pressure change on the eastern

boundary. However, there is a good physical reason to ignore variations of this form when looking at the overturning circulation: overturning represents flows in different directions at different depths, rather than a uniform direction at all depths. Uniform flows can occur, as a result of the flow through Bering Strait, or on shorter time scales to balance accumulations of mass in the North Atlantic and Arctic, but monitoring such flows is not the prime objective of this study. Accordingly, we can filter both the depth-integrated meridional transport and the spurious meridional transport due to basin-wide modes by considering not the full boundary pressure p_W, but the residual $p'_W = p_W - \overline{p_W}$, where $\overline{p_W}$ is the depth-average of p_W. This depth-average is simply defined as

$$\overline{p_W} = \frac{1}{H} \int_{-H}^{0} p_W(z)\, dz. \tag{7}$$

In removing this depth-average, we are in fact removing a legitimate component of the overturning circulation since, even with no net northward flow through a section, there must be a net geostrophic flow to balance the Ekman transport. This is simple to add back in if it is desirable to do so (assuming Ekman transport is dominated by that due to surface wind stress), since the Ekman component is near the surface, and the missing geostrophic component is by definition uniform with depth (irrespective of whether the true dynamical response to wind stress produces a depth-independent meridional transport). Note that, in ignoring changes of depth-averaged bottom pressure, we simplify the monitoring problem, because we now only need to know the difference of pressure between one depth and another. In the case of a vertical sidewall, this could be derived using hydrostatic balance from density at the sidewall alone. When the sidewall slopes, more information is needed (the geostrophic bottom current).

Finally, it is important to consider the influence of topography, such as the Mid-Atlantic Ridge, away from the ocean boundaries. Equation (2) assumes that no there is no topography intervening between the boundary pressures p_W and p_E. More generally, we should consider the sum of the zonal integrals over each ocean section at a particular depth, and the difference in boundary pressures across each intervening piece of topography then enters into the equation. In fact, as the Appendix shows, intervening topography is only significant at depths which are blocked over a wide range of latitudes, hence the division in Figure 1 of levels below the peak of the ridge into "weakly blocked" and "blocked" depths.

To summarise: east minus west pressure differences should give a good measure of meridional transport at a given depth. We expect most of the variation of pressure along depth contours to occur on the western boundary, because such variations are associated with strong depth-integrated flows such as occur in western boundary currents. Variations in bottom pressure which are constant along depth contours can equally well occur at eastern or western boundaries, potentially causing a problem for a monitoring effort focused only at the western boundary. A part of this problem can be removed by ignoring the net northward transport across the section, focusing only on the overturning, but it remains to be seen whether spurious depth-dependent transports remain. Mid-ocean topography complicates the picture, but only topography which blocks a particular depth over a large range of latitudes to each side of the chosen monitoring section is likely to be a problem.

We now proceed to examine how these theoretical ideas play out in the context of an eddy-permitting ocean model, to make a realistic estimate of the effect of quantities neglected in our analysis.

3. The nature of OCCAM variability at 42°N

The main results of this paper are based on an analysis of the Ocean Circulation and Climate Advanced Modelling project model (OCCAM) run at the National Oceanography Centre, Southampton. OCCAM is a global, z-level, free surface model with a rotated grid over the North Atlantic, and is forced with NCEP reanalysis products. The model includes a coupled sea-ice component. The run we are considering (run 202) is at 0.25 degree resolution, with 66 vertical levels, and covers the 19-year period 1985-2003, following an initial 4 years of spin-up. Further details of the model formulation can be found in *Coward and de Cuevas* [2005]. The model output is supplied as five day means from which we diagnose bottom pressure and the meridional transport.

Following [*Greatbatch*, 1994] the bottom pressure anomalies diagnosed from the model are corrected by adding a spatial constant at each timestep to ensure the total mass anomaly remains zero. This is equivalent to adding a uniform layer of water to the ocean at each timestep to ensure ocean mass is conserved. This is necessary because OCCAM is a Boussinesq model which conserves volume rather than mass. Consequently, a net change in the density of the fixed ocean volume appears as a net mass change. Because oceanic mass is conserved potential effects of bottom pressure variations due to actual fluxes into and out of the ocean due to, among other things, precipitation/evaporation, river run-off, ice-melt are not represented. This is not an issue however, since, as described

below, uniform bottom pressure variability, as would result from such fluxes, only enters into our analysis as a problem which is easily overcome.

We start by examining the nature of the meridional transport variability at 42°N. The zonal-integral calculation is complicated by the rotated North Atlantic grid which deforms lines of latitude into arcs of latitude. Interpolating the velocities fields onto a regular lat-lon grid to simplify the calculation results in a significant loss of volume conservation, so instead the zonal integral of meridional transport is computed over the faces of the rotated tracer grid cells that lie on the required latitude arc. A further complication arises from the fact that the bottom grid cells are of variable depth. To account for this the velocities are interpolated to 10m bins in such a way as to preserve the volume conservation of the water column beneath each surface grid cell.

The zonally integrated meridional transport (Figure 2a) shows that at 42°N the meridional transport consists of a northward flowing upper layer between the surface and 1000m, a southward flowing layer between 1000m to 3000m, and a much weaker northward flowing layer between 3000m to 4800m. In terms of the conventional picture of an upper overturning cell and a weaker, lower overturning cell the middle layer consists of southward flowing parts of both cells with the boundary between them lying at a depth of 2600m. The depth of the layer interfaces, particularly between the upper and middle layers, remain almost constant throughout the model integration. The mean northward transport in the upper layer is 16.7Sv, with a standard deviation of 3.1Sv. Subtracting the time-mean from the absolute transport reveals the more complex structure of the anomalous meridional transport (Figures 2b and 2c). There is a clear low-frequency mode of variability, with the transport in the upper layer, after an initial decrease, rising by 3Sv over a period of

5 years from 1987. Following this there is a steady decline by a similar amount over the remainder of the model integration. These changes in the northward flow are balanced by corresponding changes in the southward flow below. As shown in *Bingham et al.* [2007], this low-frequency mode is the dominant feature of the meridional transport at latitudes north of 40N.

While these meridional transport fluctuations generally lie within the layers defined by the absolute meridional transport, the depth of the zero point of the transport fluctuations is somewhat lower, with a mean depth of about 1300m, although this depth varies slightly according to the amplitude of the fluctuations. Imposed on top of the inter-annual mode of variability is a seasonal cycle with an amplitude between 0.5Sv to 1Sv, and higher frequency variability of comparable amplitude. Meridional transport variability from 3000m to 4800m is of similar, or greater, magnitude than the mean meridional transport but is not clearly related to the mean structure of the lower cell. Rather, it is dominated by high-frequency variability that is depth-independent. Depths greater than 4800m are defined only for a channel in the far east of the basin (see Figure 6). Here the flow is extremely weak, leading to the sharp change in magnitude at 4800m in Figure 2b.

It is difficult to say much regarding the realism of the MOC variability over the period studied given the lack of observations. *Marsh et al.* [2008] find that OCCAM MOC strength at selected WOCE sections in the North Atlantic agree with published observations within their, admittedly large, error bars. In addition, the seasonal and intra-annual variability are not unreasonable when compared with the first observations from 26°N [*Cunningham et al.*, 2007; *Kanzow et al.*, 2007]. More generally, *Marsh et al.* [2008] finds

that the variability of OCCAM's sea surface temperature and North Atlantic heat content compares well with satellite and in-situ observations.

As described in section 2 we expect there to be a strong relationship between the meridional transport variability as shown in Figure 2 and bottom pressure (bottom pressure) variability at this latitude, particularly on the western boundary. Figure 3 shows that bottom pressure variability at 42°N is greatest on the western side of the basin. (Throughout this paper bottom pressure is expresses as an equivalent water thickness $h = p_b/g\rho_0$, where ρ_0 is the mean density of seawater and g is acceleration due to gravity.) For the unfiltered bottom pressure (black line) the standard deviation on the western boundary is about 5.5cm. Beyond the shelf this rapidly falls to an average standard deviation of about 1cm in the interior.

A Fast Fourier Transform filtering method is used to partition the variability into high- (periods less than 100 days), mid- (periods between 100 and 400 days), and low- (periods greater than 400 days) frequency bands. To avoid Gibbs ringing, the Fourier coefficients at the end points of each frequency band are tapered using a cosine bell curve centred on the cut-off point, and whose width is one-fifth the cut-off wavelength. These frequency bands, and filtering method, will be used throughout the paper when referring the high-, mid-, and low-frequency variability of any quantity.

Having thus partitioned the bottom pressure variability we find that the dramatic difference between the shelf and the interior is primarily due to the characteristics of the high-frequency variability (red line). For the mid- and low-frequency bottom pressure variability the difference between the shelf and deep ocean, although smaller, is still pronounced, with both bands having a standard deviation of 2cm on the shelf and an average

standard deviation of 0.5cm in the interior. In all cases there is a small downward trend from west to east across the basin, with local deviations associated with topography.

Above we saw that meridional transport variability at 42°N has a clear low-frequency mode and therefore we now examine more closely the temporal and spatial structure of low-frequency bottom pressure variability across the North Atlantic at 42°N (see Figure 4). We have seen how the northward transport in the upper cell occurs in the depth range 0-1300m, and the return flow is in the 1300-3000m depth range. These isobaths are marked on the eastern and western slope panels in Figure 4, as is the 340m isobath, which defines the shelf edge. On the western slope the bottom pressure on the shelf and its weaker projection onto the upper slope to 1300m, shows the same low-frequency signal as does the meridional transport, but in the opposite sense. Bottom pressure declines to a minimum in the mid-1990s and then begins an upward trend over the remainder of the model run. On the lower slope below the 1300m isobath, in the depth range that corresponds to the compensating meridional transport variability in the lower layer, the same low-frequency bottom pressure mode is also seen but with the sign reversed.

From theory, meridional transport variability is determined by the difference between bottom pressure in these depth-intervals on the western boundary and the bottom pressure variability in the corresponding depth-intervals on the eastern boundary (ignoring for a moment any intervening topography). Figure 4b shows that apart from on the shelf above 340m, the bottom pressure signals on the eastern slope in the 340m to 1300m depth range and 1300m to 3000m depth range are weak, much weaker than the corresponding bottom pressure signals on the west. From this we can expect that meridional transport variability can be determined quite accurately using bottom pressure on the western boundary only.

However, since at this latitude the Mid-Atlantic Ridge (MAR) intersects the basin in the 1800m to 3000m range we still need to consider bottom pressure on the flanks of the MAR because it will be the pressure difference between eastern slope and eastern flank of the MAR together with pressure difference between western slope and western flank of the MAR that will determine the true meridional transport in the 1800-3000m depth range. However inspection of Figure 4c shows that bottom pressure variability is almost symmetrical about the peak of the MAR. The consequence of this is that pressure gradient fluctuations on one side of the MAR are cancelled by those on the other. Hence, we can anticipate that neglecting the MAR will make little difference to our calculation of the meridional transport. And indeed, this is what we find below. Referring to the theory provided in the appendix this is to be expected because the 3000m contour at 42°N is only "weakly blocked" (see Figure 7).

Figures 4(e-h) show the low-frequency SSH field across 42°N from the model for comparison with model bottom pressure. The nature of SSH variability across much of the basin is generally quite different from that of bottom pressure, particularly between the western shelf and 32W which defines the western flank of the MAR, indicating the importance of baroclinic processes on these timescales in this region. To a lesser extent the same is also true to the east of 32W. This is because SSH variability reflects both barotropic processes, which have an equal magnitude in both bottom pressure and SSH, and baroclinic process, which have a much greater SSH than bottom pressure signature (for instance, for the first baroclinic mode, which has the greatest baroclinic bottom pressure signature, the ratio is approximately 0.1 in a flat-bottomed ocean, and less with topography [*Rhines*, 1970]). However, we see that on the eastern and western shelves (above 340m) the bottom

pressure and SSH are very similar. Strong coupling between bottom pressure and SSH in shallow regions appears to be a general feature of ocean models [*Vinogradova et al.*, 2007; *Bingham and Hughes*, 2008].

We also see how the western slope prevents much of the variability seen in the deep ocean from being communicated onto the shelf where the timeseries is characteristic of the dominant interannual mode of meridional transport variability described above. Moreover, this interannual meridional transport signature is absent on the eastern shelf, with the variability being in general rather weaker than it this on the western shelf, and continuous with the variability in deeper water. A similar difference between the variability on the eastern and western shelves is also clear in the SSH variability across 42°N observed from altimetry (Figure 5), as is the decoupling of the SSH signal across the western slope, and the lack of such decoupling across the eastern slope, which suggests little interaction of the eastern signals with topography, and hence small bottom pressure signals on the slope. Significant low-frequency power has also been seen in tide gauge records from along the U.S. east coast [*Maul and Hanson*, 1991; *Unal and Ghil*, 1995], while, as *Hakkinen* [2001] has also pointed out, such low-frequency power is lacking in the open ocean.

These similarities between observations and the model strongly suggest, as does theory, that the negligible interannual bottom pressure variability on the eastern boundary and strong interannual variability on the western boundary is a realistic feature of the ocean and not just a model artefact and support our case that interannual meridional transport variability can be determined using only western boundary observations.

4. The geostrophic calculation

Having established in a qualitative fashion the nature of bottom pressure variability at 42°N and its relationship to the meridional transport we now complete a more rigorous test of the geostrophic meridional transport calculation. To facilitate a comparison between the actual meridional transport, determined from the model velocities in 10m depth-intervals, and the meridional transport computed from geostrophy, the boundary pressure at the mid-points of the same depth-intervals was calculated. These were then used to determine the geostrophic transport between each pair of points at each level. The topography across 42°N as it appears in the model is shown in Figure 6, with the points used in the geostrophic calculation shown coloured. In the actual ocean, slopes will almost always be finite so the boundary pressure is also a bottom pressure. However, because the model has insufficient resolution to resolve steep slopes these appear in the model as vertical walls, and so the model boundary pressures are generally not true bottom pressures.

To test the hypothesis that the actual meridional transport, T, can be determined with adequate accuracy using only pressure on the western boundary we shall examine four primary cases: T_{all}, the full geostrophic calculation using all east-west pressure differences at each depth (that is, using pressure at all of the coloured boundary points in Figure 6); T_{ew}, the geostrophic calculation using only the pressure difference between the easternmost and westernmost boundaries at each depth (that is, using pressure only at the red and blue boundary points in Figure 6); T_w, the geostrophic calculation using only the pressure on the western boundary (that is, using pressure only at the blue boundary points in Figure 6); T_e, the geostrophic calculation using only the pressure on the eastern boundary (that is, using pressure only at the red boundary points in Figure 6). For reasons that will

become clear we also consider the additional case T'_w, which is the geostrophic calculation using only the pressure on the western boundary but where the depth-average boundary pressure has been removed. For completeness we also include the analogous case for the eastern boundary, T'_e.

Both correlation and skill are used to asses the performance of the calculations relative to the directly computed transport. Unlike correlation, skill, which here is defined as

$$s = 1 - \mathrm{var}(T - T_*)/\mathrm{var}(T), \tag{8}$$

where $\mathrm{var}(X)$ represents the variance of timeseries X and $*$ signifies $all, ew, \mathrm{or} w$, also takes into account the amplitude of the variability. Clearly, a perfect computation will have a skill of 1, meaning T_* captures 100% of the variance in the actual timeseries.

The results of the geostrophic calculation for the six cases described above are shown in the left-hand column of Figure 8, while the corresponding error fields, defined as $T - T_*$, are shown in the right-hand column. The performance of those cases that include the western boundary is assessed in Figure 9 where the correlation and skill scores as a function of depth are shown.

T_{all} establishes the baseline against which the subsequent approximations can be judged. Panels (a) and (g) of Figure 8 show that when all east-west pressure differences are taken into account the meridional transport is generally well determined. It is not perfectly determined, however, as indicated by the non-zero residual. In the upper few hundred metres the actual meridional transport includes a significant Ekman component not determined by geostrophy. Smaller discrepancies are also found below the Ekman layer. These deviations from the actual transport are reflected in the less than perfect correlation and skill scores for T_{all} (red curves in panels (a) and (b) of Figure 9), which range from ef-

fectively zero above 100m and below 4800m, to a maximum correlation of 0.92 and skill of 85% at 500m. Above 2500m, the performance of T_{all} generally follows the strength of the transport variability, while below 2500m the performance is roughly constant with the correlation and skill scores averaging about 0.9 and 70%, respectively. The performance of T_{all} tends to follow the depth structure of the strength of the transport because where the geostrophic flow is weaker errors due to either the numerics of the calculation or small departures from geostrophy become more significant and therefore have greater power to diminish the performance measures. If we consider only the interannual component of the meridional transport, then above 3000m the skill of T_{all} is somewhat improved (panels (c) and (d) of Figure 9). Yet, below 3000m it is significantly poorer. Again, this is because the amplitude of the low-frequency variability is small and so noise in the numerics of the calculation becomes significant. This also explains the decrease in skill from 1000m to 1300m.

The first simplification of the geostrophic calculation is to ignore pressure differences due to intervening topography and use only pressure from the most easterly and westerly boundaries. It is immediately apparent from panels (b) and (h) of Figure 8 that this simplification does little to hamper the recovery of the large-scale temporal and spatial features of the meridional transport. This in agreement with the theory in section 2 and the appendix, and with the Hovmoeller diagrams of bottom pressure shown in Figure 4. Obviously, T_{all} and T_{ew} will differ only at depths where there is intervening topography, the first of which lies on the western shelf in the depth range from 100m to 200m (see Figure 6). In Figure 8h any error introduced by the neglect of this topography is obscured

by the missing Ekman transport. Its effect is clear, however, in the substantially reduced correlation and skill scores between 200m and 300m in panels (a) and (b) of Figure 9.

At greater depths, significant topographic interruptions are formed by the Mid-Atlantic Ridge, which reaches a minimum depth of 1700m at 42°N, and, in the western basin, the southern tip of the Grand Banks, which attains a minimum depth of 2500m at this latitude (see Figures 6 and 7). Comparing panels (g) and (h) of Figure 8 we find that clear differences between T_{all} and T_{ew} arise below 2500m, where neglecting the topography results in an additional high-frequency, depth-independent transport error. In panels (a) and (b) of Figure 9 we see that below 1700m the performance of T_{ew} starts to decrease relative to T_{all}, although in absolute terms it remains constant. Then, below about 2700m, the performance of T_{ew} decreases almost linearly, while the performance of T_{all} remains constant. The fact that the error in T_{ew} starts to grow significantly below 2500m, the depth to which tip of the Grand Banks reaches, suggests that it is this feature rather than the Mid-Atlantic Ridge, whose neglect introduces the largest errors into the geostrophic calculation. The constant performance of T_{all} below 2500m and the linear decrease in performance of T_{ew} are consistent with a high-frequency, depth-independent pressure difference between the western boundary and the western flank of the Grand Banks topography resulting in high-frequency depth-independent transport variations between these topographic features which are lost when the pressure on the intervening topography is neglected. Because the rest of the flow gets weaker with depth, these transport fluctuations account for an increasing fraction of the variability with depth, and therefore lead to a gradual decrease in performance of T_{ew}.

Next, we consider the case that motivates the present work and has implications for a potential future monitoring system: The ability to calculate the meridional transport at 42°N using only the western boundary pressure. Confirming our theoretical suspicions, it is quite clear from panels (c) and (i) of Figure 8 that using the western boundary pressure we can recover much of the depth and temporal structure and amplitude of the meridional transport at 42°N. The effect of neglecting pressure on the eastern boundary is seen more clearly by comparing the residuals in panels (h) and (i). The additional error introduced by this further simplification takes the form of largely depth-independent, high-frequency transport fluctuations. Because of this additional error T_w performs significantly worse than T_{all} and T_{ew} (see panels (a) and (b) of Figure 9). Peaks in performance are found at 500m and at 2500m, where transport variability is greatest, but the skill is never greater than 50%, and is generally much lower. However, because the error is generally confined to intra-annual to annual periods, the interannual performance of T_w is much better, with the correlation and skill being much closer to that achieved by T_{all} and T_{ew} (see panels (c) and (d) of Figure 9).

In contrast to T_w, in panels (d) and (j) of Figure 8 we see that T_e bears little resemblance to the actual meridional transport, confirming that nearly all the information regarding the interannual meridional transport variability is contained on the western boundary.

There is a clear correspondence between T_e and the form of the error in T_w. Recalling that the scaling of pressure to obtain T_w and T_e differs by a factor of -1, we see that the similarities in panels (d) and (i) must result from similar depth-independent pressure signals on the eastern and western boundaries. This close correspondence, over all but the highest frequencies, is illustrated in Figure 10a, which shows the depth-average pressure

from each boundary. The correlation between these two timeseries is 0.70, and from our earlier discussion, we may suspect a basin-scale bottom pressure mode as being responsible this high correlation. Using pressure from both the eastern and western boundaries when calculating T_{ew} ensures that these depth-averages will largely cancel each other. However, using pressure from one boundary only, as is done for the T_w and T_e calculations, results in an apparent depth-independent pressure gradient (relative to a zero pressure on the neglected boundary) and corresponding erroneous depth-independent meridional transport signal.

The obvious solution to this problem is to remove the depth-average western boundary pressure prior to computing the meridional transport. This brings us to case T'_w. Comparison of the residuals for T_w and T'_w (panels (i) and (k) of Figure 8) shows that removing the depth-average pressure does reduce the amplitude of the error in the geostrophic calculation of meridional transport using only western boundary pressure. While the correlation does not change much (because it is dominated by the low-frequency correspondence between the timeseries), there is a significant improvement in the skill, particularly in the depth range 1000–2500m. Yet T'_w is still somewhat less successful than either T_{all} or T_{ew}. Again, these differences arise at primarily at high-frequencies. As a result the interannual performance of T'_w over depths less than 3000m of is not significantly different from T_{all} or T_{ew} (see panels (c) and (d) of Figure 9). Because the basin-scale bottom pressure fluctuations have the greatest affect at intra-annual periods removal of the depth-average boundary pressure acts to smooth the T'_w timeseries.

Sime et al. [2006] describe how much of the transport in the Ekman layer is compensated by an opposing depth-independent geostrophic transport, in what they refer to as the

external mode. Figure 10b shows that this balance also holds at 42°N in OCCAM; the meridional transport in the Ekman layer (blue line), which we have taken to be from the surface to 140m, is largely balanced, by the integral of meridional transport from 140m to the bottom (black line; scaled by -1). The correlation between the two timeseries is 0.76. The Ekman transport is not associated with an east-west pressure gradient. Being geostrophic, however, the depth-integrated compensation of the Ekman transport must be associated with a depth-independent pressure difference across the basin. And, indeed, the transport computed from the depth-integral of the east-west pressure difference and the directly calculated depth-integral transport are correlated at 0.67.

So we see that there are two processes leading to depth-independent boundary pressures variations: the first, basin-scale pressure variations, which produce identical changes at each boundary, and therefore have no associated transport variability; the second, the depth-independent geostrophic compensation of the Ekman layer transport, which leads to relatively small differences in the eastern and western depth-independent pressures. While the apparent east-west difference caused by neglecting the eastern boundary can be compensated by removing the depth-average pressure from the western boundary, the geostrophic compensations of the Ekman transport cannot be recovered using only the western boundary pressure.

In addition to the depth-independent pressure signal on the eastern boundary there is also a seasonally repeating signal (see Figure 8f). This represents a further error in the calculation of meridional transport using only western boundary pressure, which, together with the missing geostrophic compensation of the Ekman transport, explains why T'_w, although an improvement over T_w, still does perform as well as T_{all} or T_{ew}

when considered over the full frequency spectrum. The residual signal on the eastern boundary places a limit on the temporal resolution of the meridional transport calculated using western boundary pressure: only interannual or longer periods may be reliably determined.

From Figure 2b it is clear that the dominant interannual mode of meridional transport variability can be characterised as consisting of an upper layer above 1300m balanced by a deeper layer to a depth of 3000m. For an overall assessment of the geostrophic calculation we therefore compare, for each of the six cases described above, the depth-integrals of T and T_* over the upper layer interval 100m to 1300m (denoted by U and U_*), and the lower layer interval 1300m to 3000m (denoted by L and L_*). The upper layer starts at 100m to exclude the Ekman layer transport which will not be determined by the geostrophic calculations. U_* and L_* and for each of the four cases that include the western boundary are shown in the left-hand and right-hand columns, respectively, of Figure 11. We include both correlation and skill relative to the directly computed transport as measures of performance. However, skill is the more relevant in this context and so we shall focus on this in the discussion.

Focusing first on the upper layer we find that using all pressure differences we can recover 79% of the total variance (panel a). Deviations from the actual transport are concentrated at the highest frequencies, and so at interannual timescales 92% of the variance is recovered. Neglecting intervening topography, which, as described earlier, in this depth range only occurs on the western shelf, reduces the skill of the geostrophic computation to 66% (panel b). Comparing the U_{all} and U_{ew} timeseries we that this reduction in skill is due primarily to spurious high-frequencies. These arise because local pressure fluctua-

tions in the narrow westernmost channel are not balanced when intervening topography is ignored. At sub-annual frequencies, however, the skill of U_{ew} is 92%, identical to the skill of U_{all}.

Given the spurious pressure gradient and corresponding error in U_{ew} introduced by the channel on the western shelf, when calculating U_w (panel c) we use, within the depth range spanned by the channel, the pressure on the edge of the continental slope rather than at the most westerly boundary. (Something that would obviously be done in practice.) This adjustment results in a small improvement in the scores compared with using the actual westernmost boundary points. Yet, due to the basin-scale pressure signals described above, the skill of U_w is still only 17%. Because the basin-scale pressure signals have most power at annual or shorter periods the low-frequency skill of U_w is much better (79%). As before, we see that subtracting the depth-average boundary pressure significantly reduces the spurious high-frequency transport signal (panel e), increasing the skill of the western boundary calculation to 46% for the full signal and 92% for the interannual signal, identical to the skill obtained when using all east-west pressure differences.

The pattern for the upper layer calculations is repeated for the lower layer with the skill becoming progressively worse as we first neglect intervening topography and then the pressure on the eastern boundary, and then improving once the depth-average pressure is removed from the western boundary. As Figure 8b shows, errors in the geostrophic calculating grow with depth and this is reflected in the slightly lower skill scores for L_{all} and L_{ew} compared with the corresponding upper layer calculations. Given that neglecting the eastern boundary introduces a depth-independent error we might expect the skill of L_w to be lower than U_w since the lower layer is thicker. Yet, in fact, the skill of L_w is

slightly greater. This is because U_w also includes an error due to the upper layer pressure signal described above, which requires balancing by the eastern boundary. This is also reflected in the greater skill of L'_w relative to U'_w. Note that, surprisingly, the interannual skill for L'_w is actually a few percent higher than the L_{all} and L_{ew} cases. A possible explanation for this is that the errors in the geostrophic calculation that persist beyond the annual period have a small non-zero depth average.

5. Discussion

The key result of this study, summarised in Figure 12, is that on timescales longer than one year variations of the North Atlantic meridional transport in the OCCAM ocean model can accurately be determined from bottom pressure on the western boundary. In the upper layer (100–1300m) at low-frequencies the skill of the meridional transport calculation using only western boundary pressure is 92%, equal to the calculation taking into account all bottom pressure pairs across the basin, and the standard deviation from the directly computed timeseries is 0.29Sv. In the lower layer (1300–3000m) the low-frequency skill is 96%, and the standard deviation from the directly computed timeseries is 0.24Sv. These results demonstrate the potential accuracy of a western boundary MOC observing system. The accuracy depends on the fact that low-frequency depth-dependent variations in bottom pressure on the eastern boundary and on the intervening topography are either negligible compared with those on the western boundary or compensating, and therefore make little contribution to the depth-dependent pressure gradient which determines the meridional transport.

In determining the meridional transport from the western boundary bottom pressure we find it necessary to remove the depth-average bottom pressure. This is due to a basin-

scale bottom pressure variability which has power at all frequencies, including interannual, and which makes an almost equal contribution to the depth-independent pressures on the eastern and western boundaries. Hence, excluding the eastern boundary from the meridional transport calculation, without removing the depth-average bottom pressure from the western boundary, results in an apparent depth-independent pressure difference and corresponding depth-independent meridional transport signal. The inability of a western boundary array to determine the depth-independent pressure difference across the basin also means that it could not determine the geostrophic compensation of the surface Ekman transport. *Kanzow et al.* [2007] shows that this component makes a large contribution to the meridional transport at intra-annual timescales, in agreement with what we find in OCCAM. It is likely these large intra-annual fluctuations in the depth-average transport do not play a important role in regulating the Earth's climate. Therefore, separating out the depth-independent transport has the advantage of acting as a low pass filter to what is essentially noise as far as detecting climatically important changes in the MOC is concerned. Of course, the Ekman transport itself and its geostrophic compensation, including any low-frequency variability that may have significance for heat transport, can still readily be inferred from satellite observations as is done at 26°N.

As with all model results, one can question their realism. While we cannot, of course, be certain that this relationship between western boundary pressure and the meridional transport holds in reality, the differing nature of variability on the eastern and western boundaries seen in the model is substantiated by observations of sea-level from altimetry and tide-gauges. Often modelling results do not translate to the real ocean because to ensure stability models are much more viscous than the real ocean. Friction, however, is

one factor that reduces the validity of the geostrophic relationship on which our results depend, so it can be said that our results hold in spite of, not because of, the high viscosity of the model. Thus, the relationship may be even stronger in the much less viscous real ocean. That said, we cannot rule out the possibility of qualitative differences in the structure and strength of the actual time-dependent circulation that mean the relationship between western boundary pressure and meridional transport variability is not as strong as it is in reality.

A further potential problem occurs if eddies in the real ocean have a stronger influence on western boundary pressure than they do in OCCAM. Only in-situ data can answer this question, but the clear influence of the continental slope suppressing the propagation of mid-ocean sea level variability in shallower water, confirmed by altimetry, suggests that OCCAM is not unrealistic in this respect.

Finally, there is the question of whether over longer periods the eastern boundary pressure remains unimportant. We intend to perform a similar analysis of 100 years of output from a climate model to address this.

While this study suggests that measurements of western boundary pressure fluctuations are sufficient to monitor the interannual variability of the Atlantic meridional transport, it does not address the practicalities of making these measurements. With currently-available technology, it is not possible to measure bottom pressure directly to the accuracy required over interannual timescales, because a combination of sensor drift and datum loss between deployments degrades the accuracy for long period variations.

The most obvious solution is a combination of satellite altimetry to determine the sea level signal, with density measurements through the water column, permitting a determi-

nation of bottom pressure from hydrostatic balance. The difficulty here is that bottom pressure variations are a small residual of two large, compensating signals from sea level and density, and the required accuracy pushes the limits of satellite altimetry (particularly given the fine spatial resolution required to distinguish sea level signals in different depths of ocean, over a steep slope).

Alternatively, since we must in any case subtract out the depth-averaged bottom pressure, we can make use of the fact that we only need to measure the down-slope gradient of bottom pressure. For a vertical slope, this only requires density measurements. For a finite slope, we also need the horizontal pressure gradient at the sea floor, measured to an accuracy which depends on the steepness of the slope. Our proposal for the next iteration of the 42°N western boundary array maintained by POL is to use near-bottom currents, determined using high vertical resolution ADCP (Acoustic Doppler Current Profiler) measurements, to supply this information via the geostrophic relationship. This approach should enable us to distinguish the relevant geostrophic currents from any bottom boundary layer flow.

Finally, the strong correlation between sea level and bottom pressure which emerges in shallow water highlights the value of tide gauge measurements as a component of the monitoring system. Although tide gauge measurements alone are probably inadequate to determine the overturning circulation, their value is strongly boosted by the fact that there are many multidecadal tide gauge records from both eastern and western boundaries of the Atlantic, making possible inferences about circulation changes since at least the middle of the 20th century.

Acknowledgments. This study was supported by the UK NERC thematic RAPID programme, NER/T/S/2002/00439 and NER/T/S/2002/00485, and represents a contribution to the Proudman Oceanographic Laboratory's "Sea-level, bottom pressure, and geodetic oceanography" Programme. For the OCCAM model data we acknowledge the efforts of Andrew Coward and Beverly de Cuevas.

Appendix

Form stress on mid-ocean topography is subject to the same relationship with depth-integrated flow as that which occurs at the boundary. For topography which acts as a substantial barrier, such as that separating the regions marked "blocked" in Figure 1, if the topography supports a significant depth-integrated transport above it then it can also support a significant form stress, meaning that the pressures on the topography make an important contribution to the zonal integral meridional transport. However, if a depth contour can be found which passes between the east and west sides of the topography without a large meridional deflection ("weakly blocked" depths in Figure 1, then the possible size of the form stress is more constrained.

Consider the balance of terms within the region depicted in Figure 13), bounded by a depth contour $z = -H_1$ and a latitude line where $f = f_0$. This represents a plan view of the topography penetrating into the "weakly blocked" region in Figure 1. From (2) and (5), the contribution of pressure differences across the topography to zonal integral transport T is given by

$$\rho f_0 \int_{-H_1}^{-H_2} T \, dz = - \int_a^b p_b H_x \, dx, \tag{9}$$

where H_2 is the depth of the shallowest topography along ab. However, we can also calculate the form stress as an integral of the bottom pressure torque over the enclosed area A:

$$\int_A J(p_b, H) \, dA = \oint p_b \nabla H \cdot \mathbf{ds} = - \int_a^b p_b H_x \, dx. \tag{10}$$

We now use $J(p_b, H) = \rho\beta V = \rho\nabla\cdot(f\mathbf{U})$, where $\mathbf{U}$ is the depth-integrated horizontal velocity, together with (9) and (10) to give

$$\rho f_0 \int_{-H_1}^{-H_2} T\,dz = \rho \int_A \nabla\cdot(f\mathbf{U})\,dA. \tag{11}$$

Now, assuming there are no mass sources so that $\nabla\cdot\mathbf{U} = 0$, the right hand side of (11) is non-zero only when there is a flow into A at a different latitude to the flow out of the area. The largest possible value of this term is then $Q\delta f$, where Q is the total flow into (and out of) A, and δf is the maximum difference in f between the northern and southern limits of A. Given this, together with (11), we see that

$$\int_{-H_1}^{-H_2} T\,dz < Q\frac{\delta f}{f_0}. \tag{12}$$

This tells us that the maximum possible meridional transport integrated over the region marked "weakly blocked" in Figure 1 is a factor $\delta f/f_0$ smaller than the depth-integrated flow above that section of topography. Adding in the effect of wind stress or mass sources simply results in the reinterpretation of $\mathbf{U}$ (and hence Q) as representing the difference of the flow from one in Sverdrup balance. Taking as an example f_0 at 42°N and δf corresponding to an extension of 5 degrees to the south (or north) gives $\delta f/f_0 = 0.10$. In this case, for every sverdrup of meridional transport supported by mid-ocean topography in the "weakly blocked" region, there would have to be at least 10 Sv of depth-integrated flow above the blocking topography. This factor means that pressure signals at mid-ocean topography are less likely to contribute strongly to the meridional transport at depths where the topography only blocks a small range of latitudes. However, there is nothing in this argument which prevents large pressure signals occurring over the topography, in which the eastern and western pressures balance producing no net form stress. This is

what would happen, for example, in a barotropic flow following f/H contours across a ridge.

The argument for expecting most of the pressure variation to occur at the western rather than the eastern boundary is that depth-integrated currents are much stronger on the west than on the east. The scaling in this Appendix shows that, in order for pressure on weakly-blocked topography to contribute significantly to the meridional transport, depth-integrated transports above that topography would have to be ten times stronger than above blocked topography such as the eastern and western boundaries, making weakly-blocked regions also unlikely to contribute strongly to the meridional transport.

References

Bingham, R. J., and C. W. Hughes (2008), The relationship between sea-level and bottom pressure variability in an eddy permitting ocean model, *Geophys. Res. Lett.*, *35*, L03602, doi:10.1029/2007GL032662.

Bingham, R. J., C. W. Hughes, V. Roussenov, and R. G. Williams (2007), Meridional coherence of the North Atlantic meridional overturning circulation, *Geophys. Res. Lett.*, *34*, L23606, doi:10.1029/2007GL031731.

Bryden, H., H. Longworth, and S. Cunningham (2005), Slowing of the Atlantic Overturning circulation at 25N, *Nature*, *438*, 655–657.

Coward, A., and B. de Cuevas (2005), The OCCAM 66 Level Model: physics, initial conditions and external forcing., *Internal report 99*, SOC, 58pp, available from *http://www.noc.soton.ac.uk/JRD/OCCAM/OCCAM-p25k66-run202.pdf*.

Cubasch, U., G. A. Meehl, G. J. Boer, R. J. Stouffer, M. Dix, A. Noda, C. A. Senior, S. Raper, and K. S. Yap (2001), *Projections of future climate change. In, Climate Change 2001: The Scientific Basis. Contribution of Working Group I to the Third Assessment Report of the Intergovernmental Panel on Climate Change, Houghton, J. T. and Y. Ding and D. J. Griggs and M. Noguer and P. J. van der Linden and X. Dai and K. Maskell and C. A. Johnson (eds.)*, p. 881 pp, Cambridge University Press, Cambridge, United Kingdom and New York, NY, USA.

Cunningham, S., et al. (2007), Temporal variability of the atlantic meridional overturning circulation at 26.5n, *Science*, *317*(5840), 935–938, doi:10.1126/science.1141304.

Gille, S. T. (1997), The Southern Ocean momentum balance: Evidence for topographic effects from numerical model output and altimeter data, *J. Phys. Oceanogr.*, *27*, 2219–

2232.

Greatbatch, R. (1994), A note on the representation of steric sea-level in models that conserve volume rather than mass, *J. Geophys. Res.*, *99*, 12,767–12,771.

Hakkinen, S. (2001), Variability in sea surface height: A qualitative measure for the meridional overturning in the North Atlantic, *J. Geophys. Res.*, *106*(C7), 13,837–13,848.

Hirschi, J., J. Baehr, J. Marotzke, J. Stark, S. Cunningham, and J.-O. Beismann (2003), A monitoring design for the Atlantic meridional overturning circulation, *Geophys. Res. Lett.*, *30*(7), 1413, doi:10.1029/2002GL016776.

Hughes, C. W., and B. A. de Cuevas (2001), Why western boundary currents in realistic oceans are inviscid: A link between form stress and bottom pressure torques, *J. Phys. Oceanogr.*, *31*, 2871–2885.

Johnson, H., and D. Marshall (2002), A theory for the surface atlantic response to thermohaline variability, *J. Phys. Oceanogr.*, *32*, 1121–1132.

Kanzow, T., et al. (2007), Observed flow compensation associated with the moc at 26.5n in the atlantic, *Science*, *317*(5840), 938–941, doi:10.1126/science.1141293.

Kawase, M. (1987), Establishment of deep ocean circulation driven by deep-water production, *J. Phys. Oceanogr.*, *17*, 2294–2317.

Marsh, R., S. A. Josey, B. A. de Cuevas, L. J. Redbourn, and G. D. Quartly (2008), Mechanisms for recent warming of the North Atlantic: Insights gained with an eddy-permitting model, *J. Geophys. Res.*, *113*, C04031, doi:10.1029/2007JC004096.

Mathers, E. L., and P. L. Woodworth (2004), A study of departures from the inverse-barometer response of sea level to air-pressure forcing at a period of 5 days, *Q. J. R. Meteorol. Soc.*, *130*, 725–738.

Maul, G. A., and K. Hanson (1991), Interannual coherence between north Atlantic atmospheric surface pressure and composite southern U.S.A. sea level, *Geophys. Res. Lett.*, *18*(4), 653–656.

Park, J. H., and D. R. Watts (2006), Near 5-day nonisostatic response of the atlantic ocean to atmospheric surface pressure deduced from sub-surface and bottom pressure measurements, *Geophys. Res. Lett.*, *33*, L12610, doi:10.1029/2006GL026304.

Ponte, R. M. (1997), Nonequilibrium response of the global ocean to the 5-day Rossby-Haurwitz wave in atmospheric surface pressure, *J. Phys. Oceanogr.*, *27*, 2158–2168.

Ponte, R. M., and R. D. Rosen (1994), Oceanic angular momentum and torques in a general circulation model, *J. Phys. Oceanogr.*, *24*, 1966–1977.

Rhines, P. (1970), Edge-, bottom-, and Rossby-waves in a rotating stratified fluid, *Geophys. Fluid Dyn.*, *1*, 273–302.

Sime, L., D. Stevens, K. Heywood, and K. Oliver (2006), A decomposition of the Atlantic meridional overturning, *J. Phys. Oceanogr.*, *36*, 2253–2270.

Stepanov, V. N., and C. W. Hughes (2006), Propagation of signals in basin-sale ocean bottom pressure from a barotropic model, *J. Geophys. Res.*, *111*, C12002, doi: 10.1029/2005JC003450.

Stevens, D., and V. Ivchenko (1997), The zonal momentum balance in an eddy resolving general circulation model of the Southern Ocean, *Q. J. R. Meteorol. Soc.*, *123*, 929–951.

Unal, Y., and M. Ghil (1995), Interannual and interdecdal oscillation patterns in sea level, *Clim. Dyn.*, *11*, 255–278.

Vellinga, M., and R. A. Wood (2002), Global climatic impacts of a collapse of the Atlantic thermohaline circulation, *Climatic Change*, *54*, 251–267.

Vinogradova, N. T., R. Ponte, , and D. Stammer (2007), Relation between sea level and bottom pressure and the vertical dependence of oceanic variability, *Geophys. Res. Lett.*, *34*, L03608, doi:10.1029/2006GL028588.

Wood, R. A., M. Vellinga, and R. Thorpe (2003), Global warming and thermohaline circulation stability, *Phil. Trans. R. Soc. Lond. A*, *361*, 1961–1975, doi: 10.1029/2005GB00210.

Figure 1. A schematic section across the North Atlantic basin showing the components of the meridional transport relative to the key topographic features. The layer marked "blocked" defines the depth range for which it is not possible to reach one flank of the topography from the other along an isobath, whereas for the "weakly blocked" depth range it is possible.

Figure 2. (a) The zonally integrated Atlantic meridional transport at 42°N in OCCAM. (b) The meridional transport with the time-mean removed. (c) Integral over the depth range 100m to 1000m of the zonally integrated anomalous transport. Red curve shows low-pass filtered version (periods greater than 400 days).

Figure 3. The standard deviation of bottom pressure variability from west to east across the Atlantic basin at 42°N in OCCAM: black, unfiltered; red, periods less 100 days; green, periods between 100 and 400 days; blue, periods greater than 400 days.

Figure 4. The low-frequency (periods greater than 400 days) variability of bottom pressure (left) and sea level (right) across the Atlantic basin at 42°N in OCCAM: (a,e) Across the entire basin; (b,f) Across the eastern shelf and continental slope; (c,g) Across the mid-Atlantic ridge; (d,h) Across the western shelf and continental slope. Contours correspond to isobaths: 340m (dashed); 1300m (solid); 3000m (dotted), except for (c,g) where the dashed line represents the peak of the mid-Atlantic ridge at 1700m.

Figure 5. The low-frequency (periods greater than 400 days) variability of observed sea level across the Atlantic basin at 42°N: (a) Across the entire basin; (b) Across the eastern shelf and continental slope; (c) Across the mid-Atlantic ridge; (d) Across the western shelf and continental slope. Contours correspond to isobaths: 340m (dashed); 1300m (solid); 3000m (dotted), except for (c) where the dashed line represents the peak of the mid-Atlantic ridge at 1700m.

Figure 6. The topography across the Atlantic at 42°N as it appears in OCCAM, with north into the page. The boundary points where pressure is used in the geostrophic calculations of the meridional transport are shown coloured. The most easterly and westerly boundary points at a given depth are red and blue, respectively. The easterly flank and westerly flank boundary points on the intervening topography are yellow and cyan, respectively.

Figure 7. The topography of the North Atlantic basin showing contours at 1300m, the depth of the interface between upper and lower layers of the meridional transport variations at 42°N (dashed line) in OCCAM , and at 3000m, the bottom of the lower layer.

Figure 8. Testing the geostrophic calculation of the Atlantic meridional transport at 42°N in OCCAM. The meridional transport computed using: (a) all pairs of east and west points (b) extreme east and west points only (i.e. ignoring intervening topography); (c) western boundary points only; (d) eastern boundary points only; (e) western boundary points with the depth-average boundary pressure removed; (f) eastern boundary points with the depth-average boundary pressure removed;. (g-l) The actual transport minus the computed transports shown in (a-f).

Figure 9. Testing the geostrophic calculation of the Atlantic meridional transport at 42°N in OCCAM: (a) Correlation of the computed transports with the actual transports as a function of depth; (b) The skill of the computed transports in accounting for the variance of the actual transports as a function of depth. All east-west pairs (red); extreme east-west points only (green); extreme west points with depth-average removed (blue); extreme west points with depth-average kept (blue dashed). (c-d) As in (a-b) but with low-pass filtering (retaining periods greater than 400 days).

Figure 10. (a) The depth-average of bottom pressure, expressed in equivalent millimetres of water thickness, on the eastern boundary (red) and western boundary (blue). (b) The zonally integrated transport from the surface to 140m, which is essentially the Ekman transport (blue). The zonally integrated transport from 140m to the bottom multiplied by -1, representing the geostrophic compensation of the Ekman transport (black). The depth-integral of the east-west pressure difference scaled by a factor of $1/\rho_0 f$ to obtain the depth-independent geostrophic transport (red). Only a subsection is shown to make clear the high-frequency correspondence between the timeseries.

Figure 11. Testing the geostrophic calculation of the Atlantic meridional transport at 42°N in OCCAM. The anomalous transport integrated over 100-1300m using: (a) all pairs of east and west points; (b) extreme east and west points only (i.e. ignoring intervening topography); (c) western boundary points only; (d) western boundary points only with the depth-average boundary pressure removed; (e-h) Repeating (a-d) for the anomalous transport integrated over 1300-3000m. In each case the total anomalous zonally integrated transport is shown in red. Low-pass filtered (periods greater than 400 days) scores are shown in brackets.

Figure 12. (a) The interannual Atlantic meridional transport variability at 42°N is OCCAM integrated over 100-1300m calculated directly (red) and determined using bottom pressure on the western boundary (blue). (b) As in (a) but for the 1300-3000m depth range.

Figure 13. A plan view of the topography penetrating into the "weakly blocked" region in Figure 1. The shaded region is bounded by the depth contour H_1 and a line of latitude that is tangent to the southern tip of the shallower depth contour H_2.

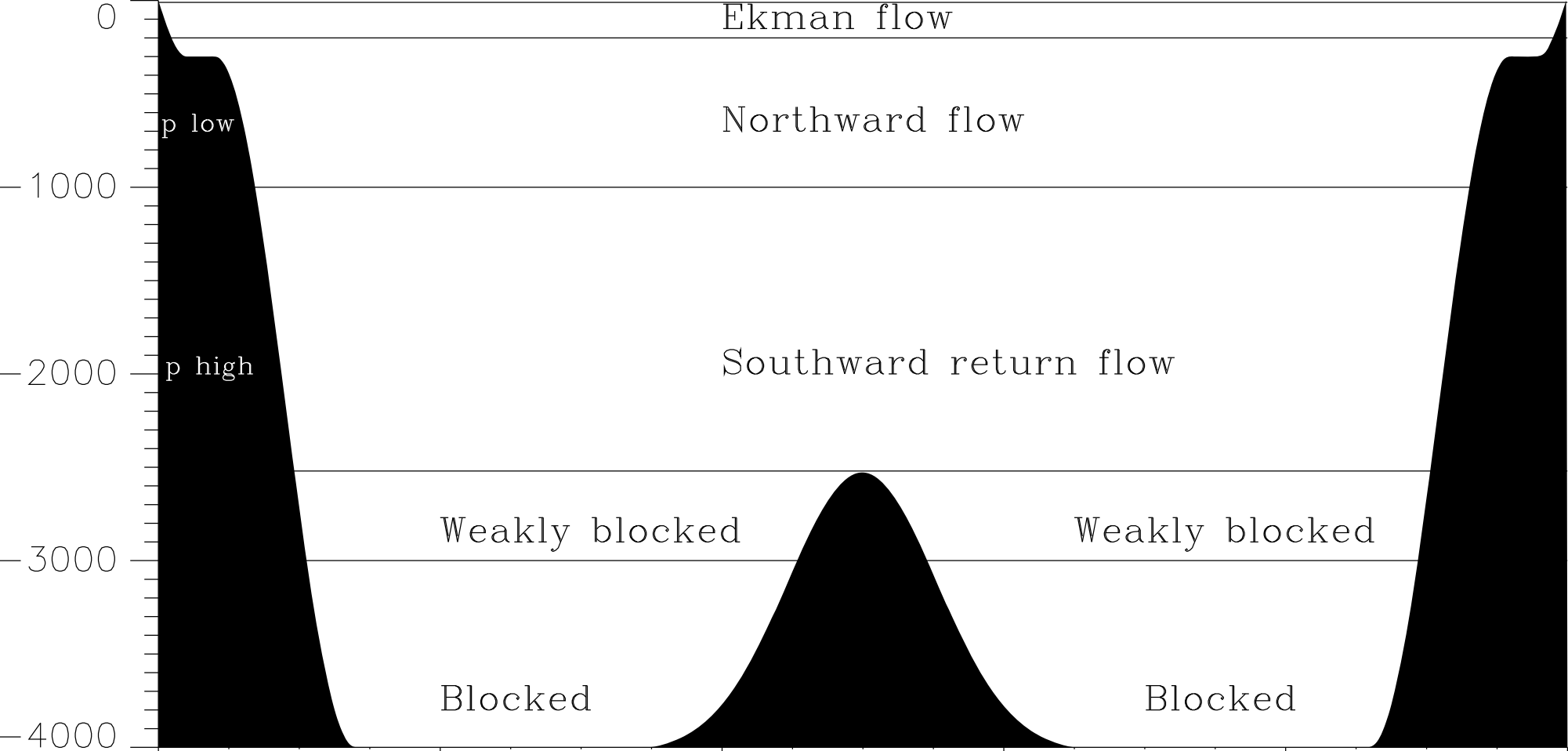
0
1000
2000
3000
4000
Ekman flow
Northward flow
Southward return flow
Weakly blocked
Weakly blocked
Blocked
Blocked
p low
p high

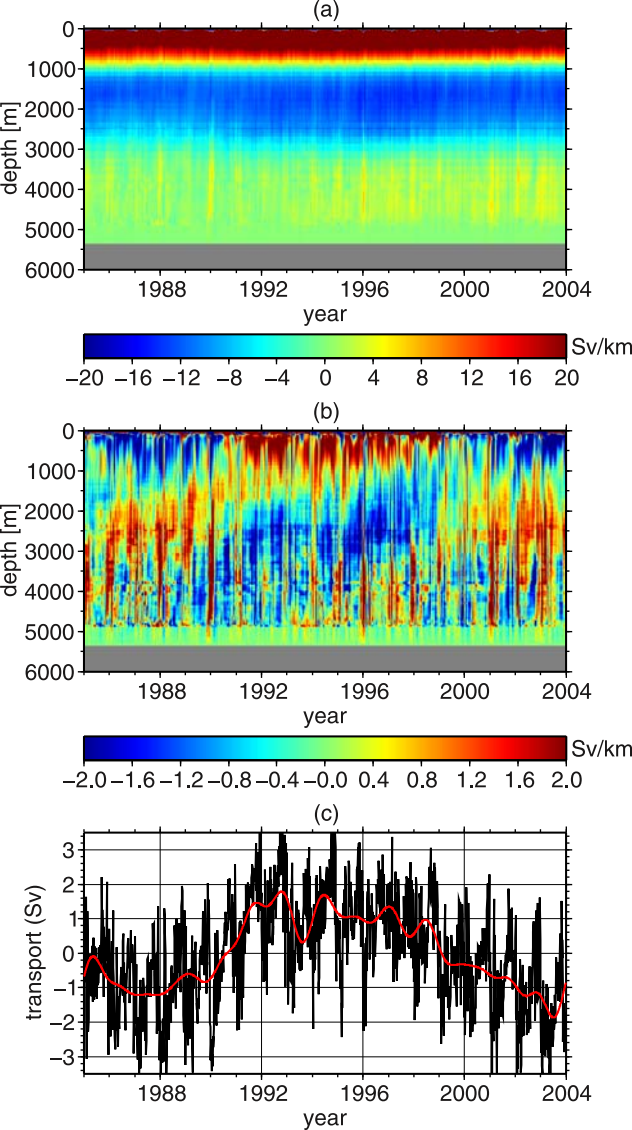
(a)
depth [m]
0
1000
2000
3000
4000
5000
6000
1988
1992
1996
2000
2004
year
Sv/km
−20 −16 −12 −8 −4 0 4 8 12 16 20
(b)
depth [m]
year
Sv/km
−2.0 −1.6 −1.2 −0.8 −0.4 −0.0 0.4 0.8 1.2 1.6 2.0
(c)
transport (Sv)
3
2
1
0
−1
−2
−3
year

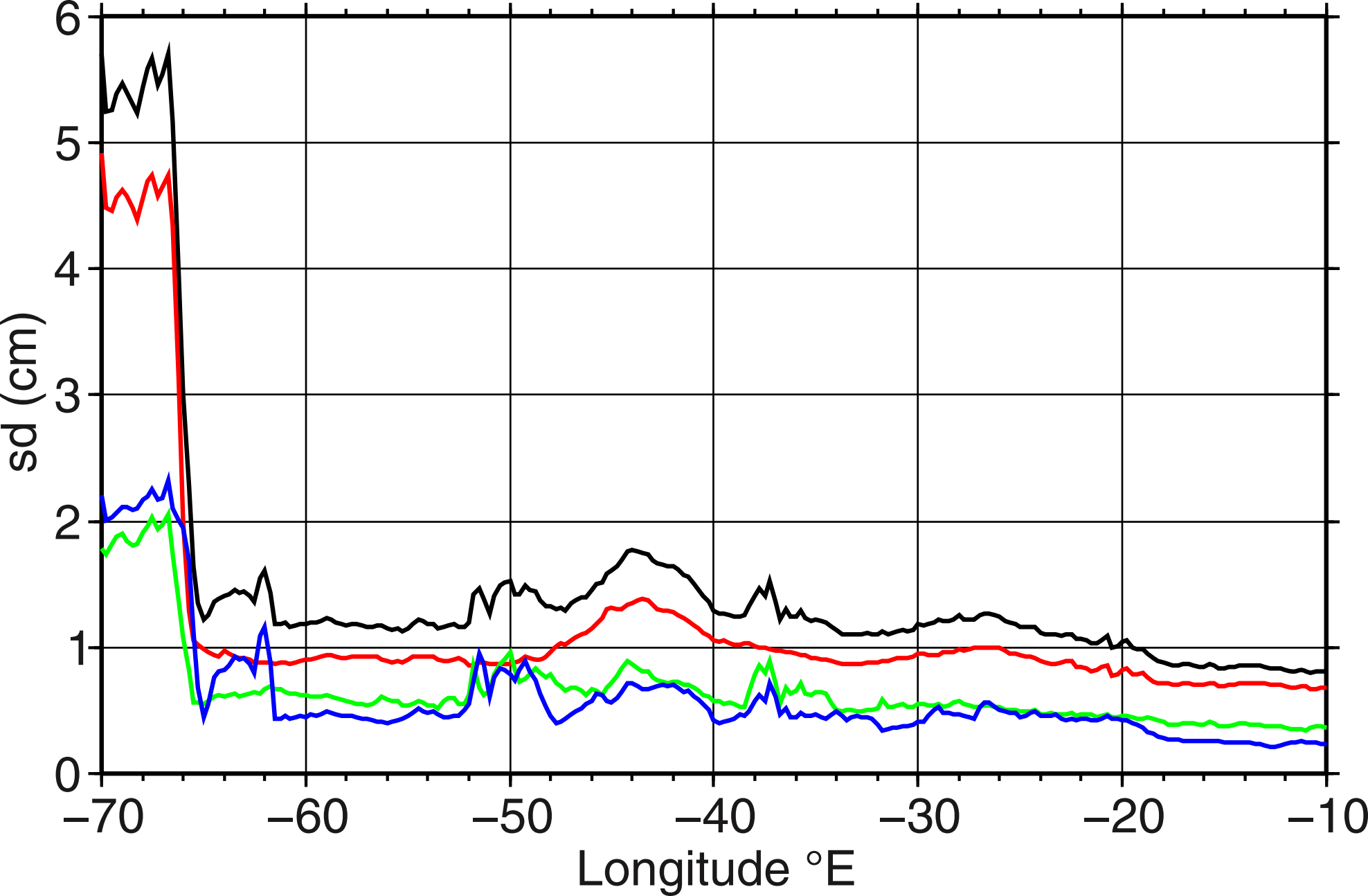
6
5
4
3
2
1
0
sd (cm)
−70
−60
−50
−40
−30
−20
−10
Longitude °E

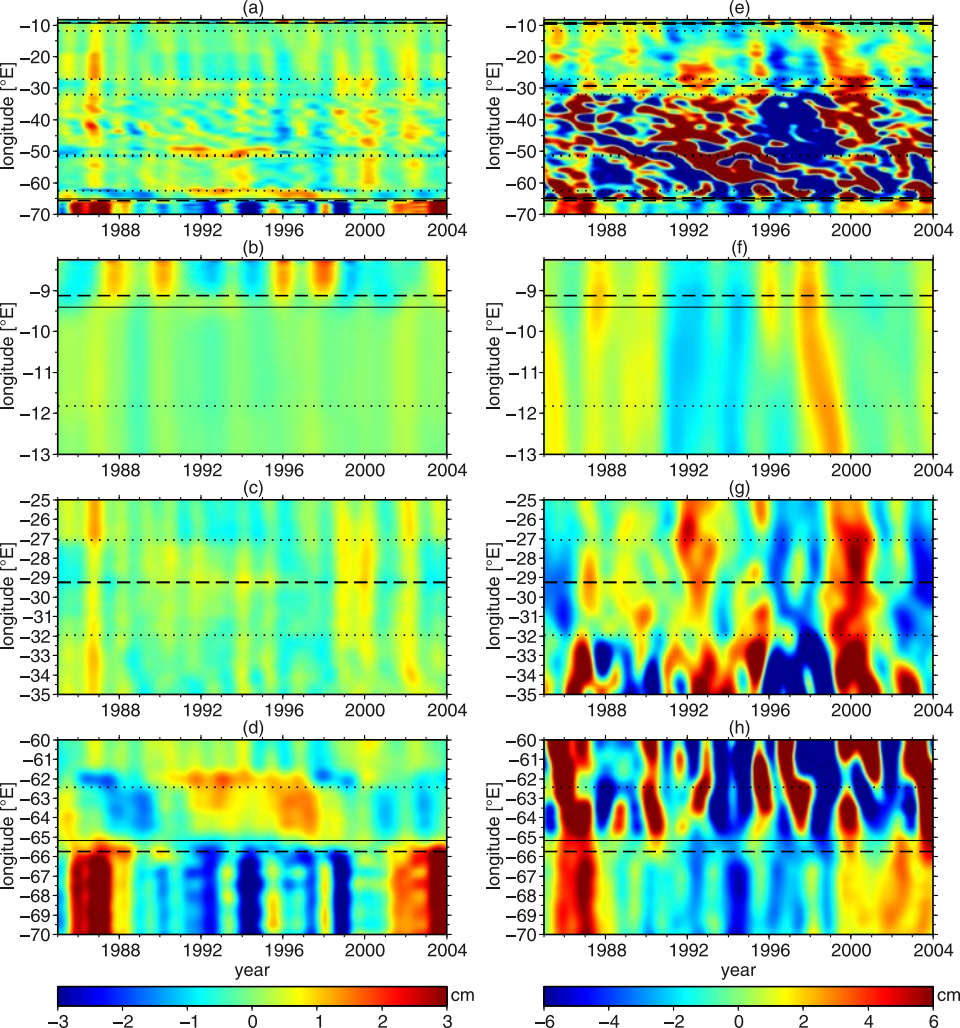
(a)
(e)
(b)
(f)
(c)
(g)
(d)
(h)
longitude [°E]
year
1988
1992
1996
2000
2004
cm
−3
−2
−1
0
1
2
3
−6
−4
−2
0
2
4
6

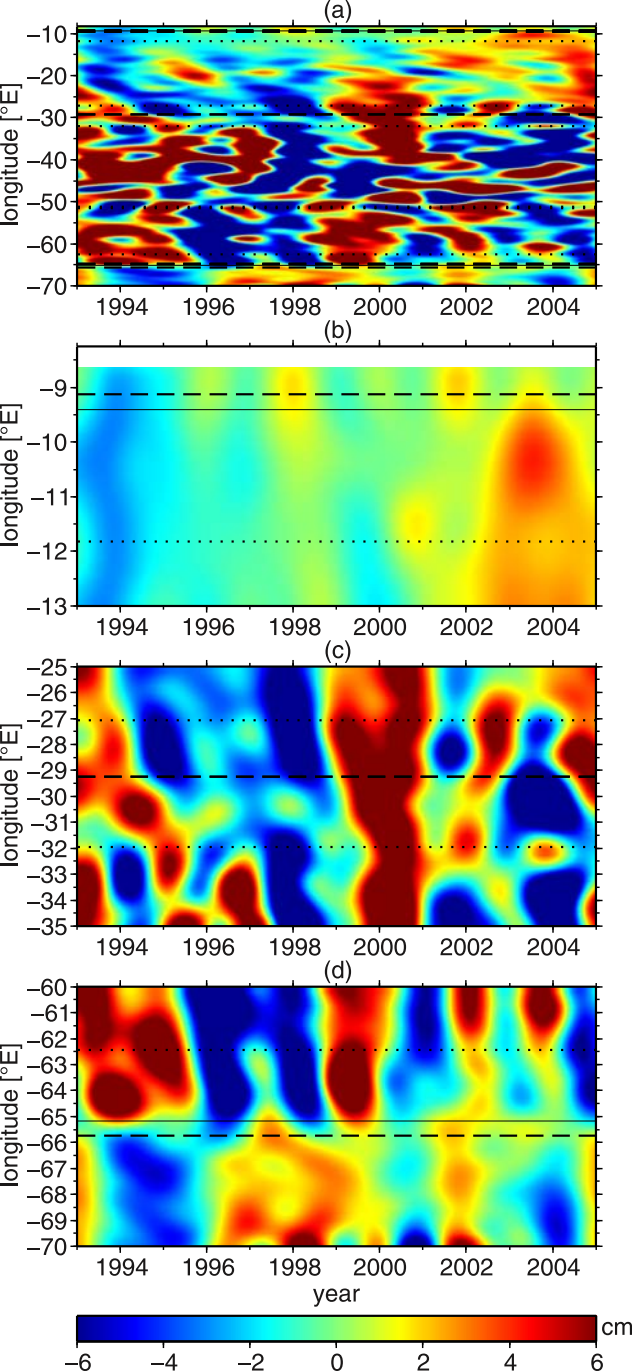
(a)
longitude [°E]
−10
−20
−30
−40
−50
−60
−70
1994
1996
1998
2000
2002
2004
(b)
longitude [°E]
−9
−10
−11
−12
−13
1994
1996
1998
2000
2002
2004
(c)
longitude [°E]
−25
−26
−27
−28
−29
−30
−31
−32
−33
−34
−35
1994
1996
1998
2000
2002
2004
(d)
longitude [°E]
−60
−61
−62
−63
−64
−65
−66
−67
−68
−69
−70
1994
1996
1998
2000
2002
2004
year
cm
−6
−4
−2
0
2
4
6

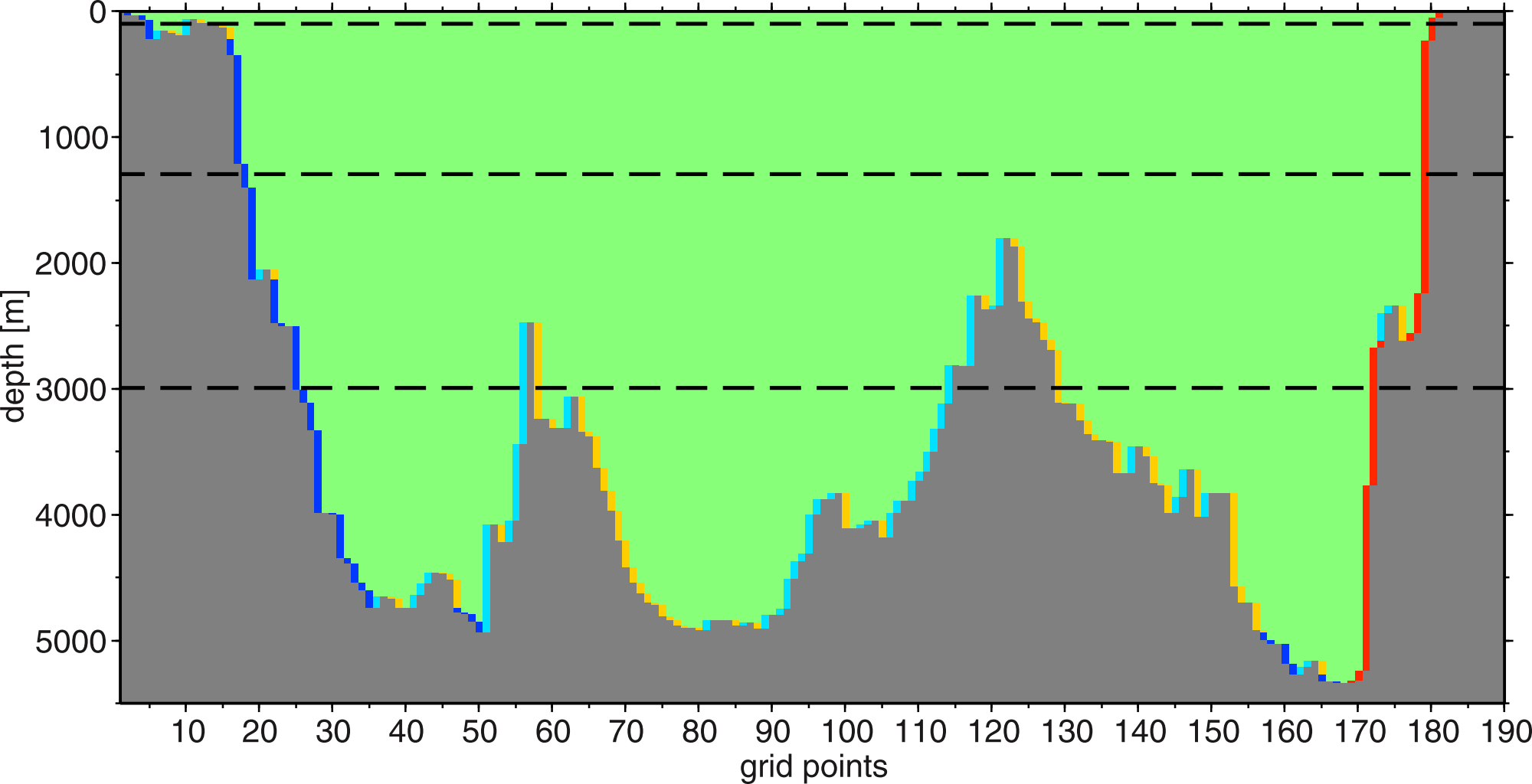
0
1000
2000
3000
4000
5000
depth [m]
10
20
30
40
50
60
70
80
90
100
110
120
130
140
150
160
170
180
190
grid points

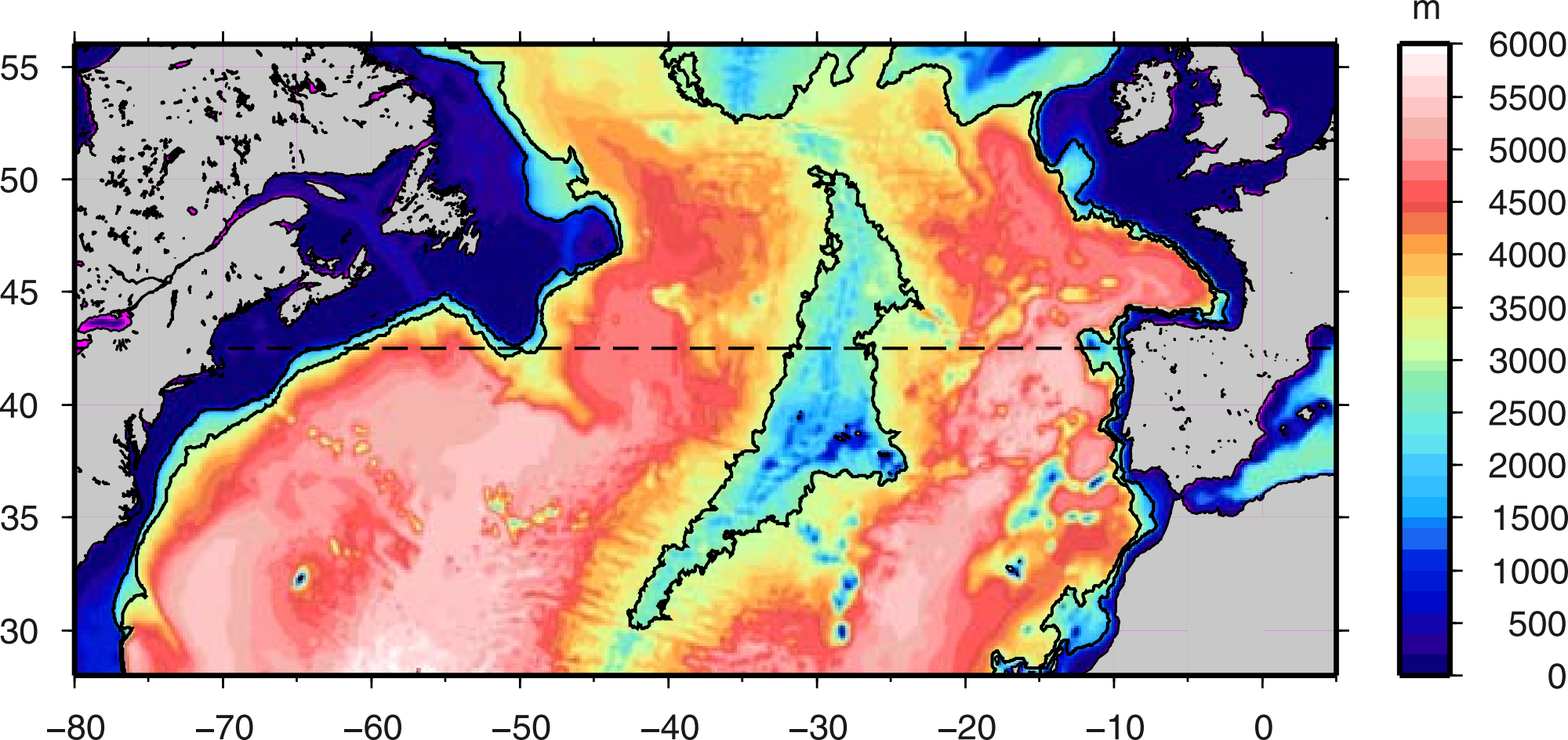
m
6000
5500
5000
4500
4000
3500
3000
2500
2000
1500
1000
500
0
55
50
45
40
35
30
−80
−70
−60
−50
−40
−30
−20
−10
0

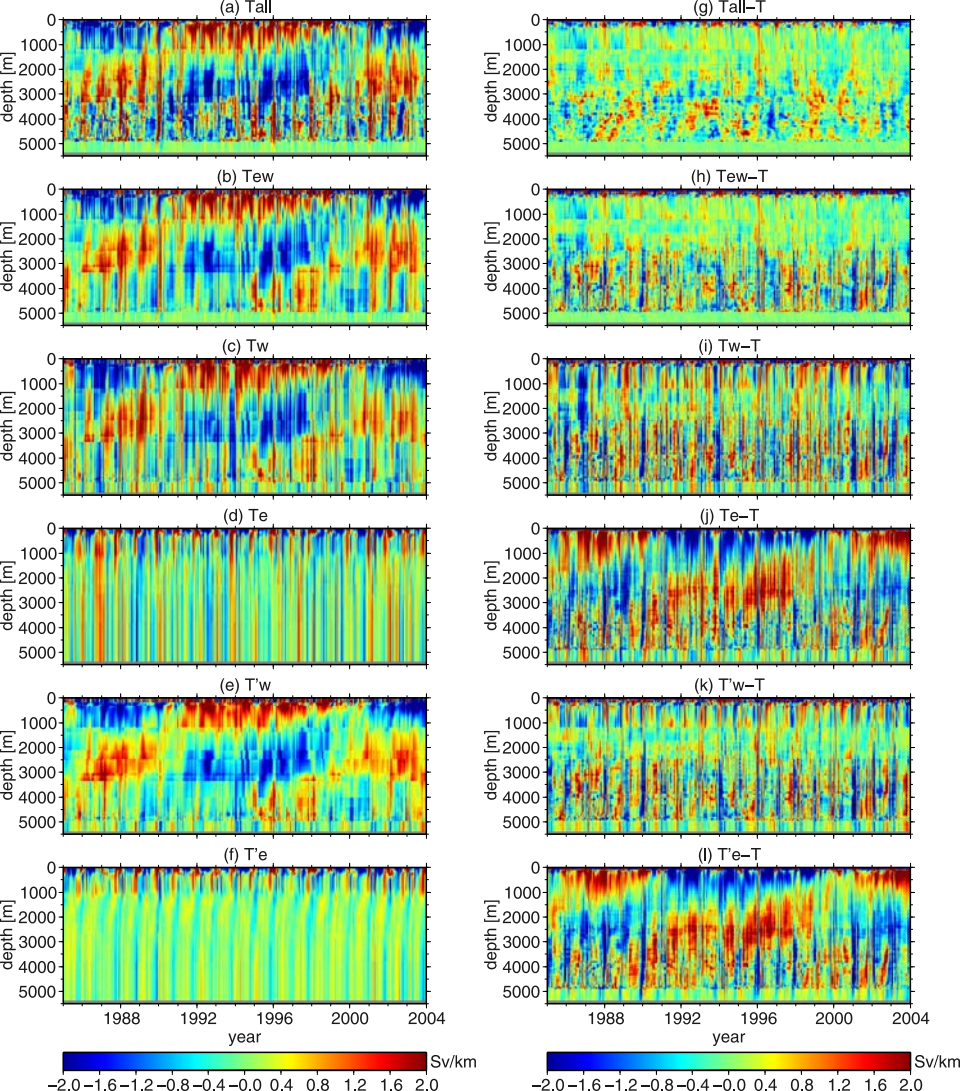
(a) Tall
(b) Tew
(c) Tw
(d) Te
(e) T'w
(f) T'e
(g) Tall−T
(h) Tew−T
(i) Tw−T
(j) Te−T
(k) T'w−T
(l) T'e−T
depth [m]
0
1000
2000
3000
4000
5000
1988
1992
1996
2000
2004
year
Sv/km
−2.0 −1.6 −1.2 −0.8 −0.4 −0.0 0.4 0.8 1.2 1.6 2.0

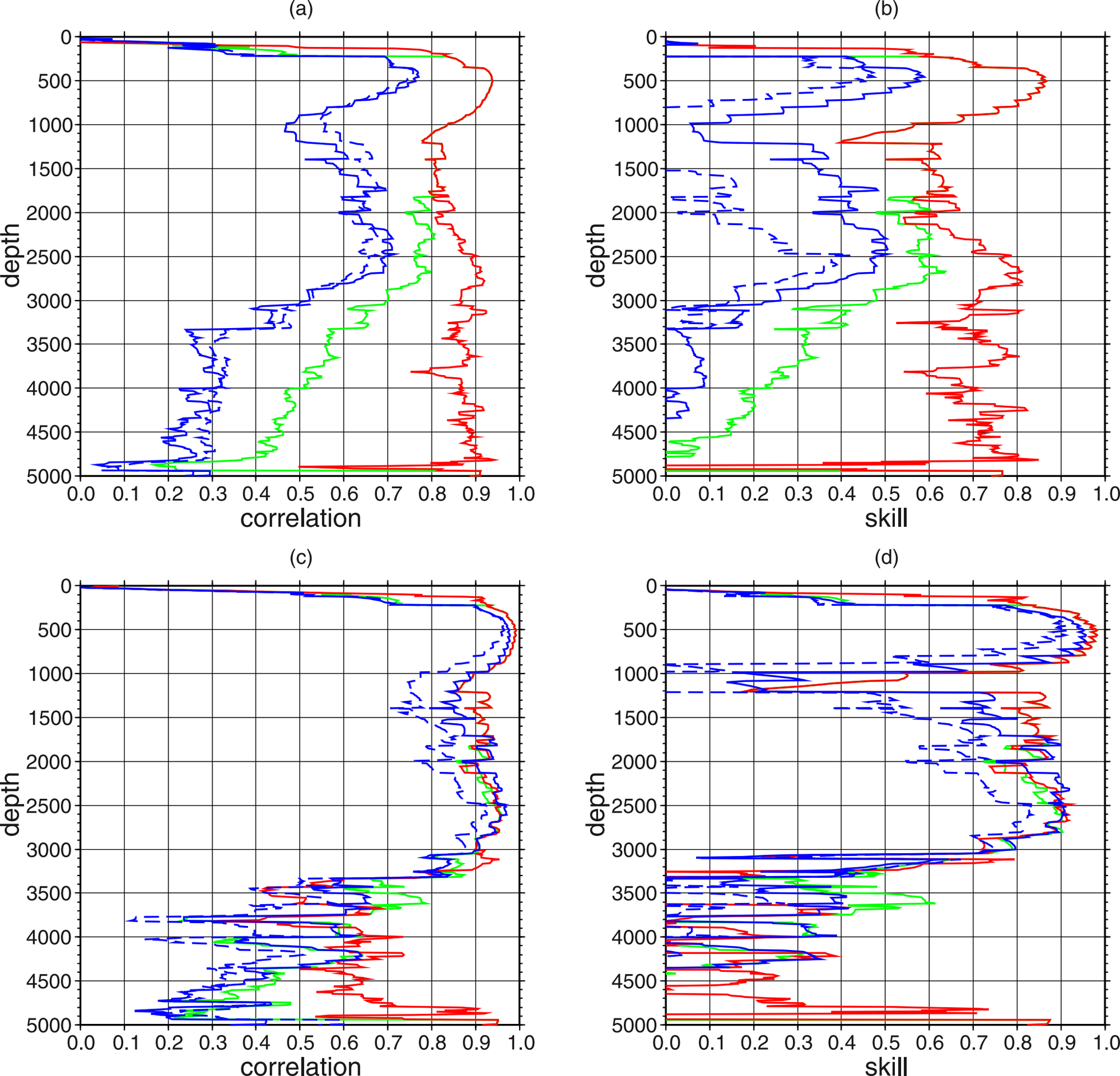
(a)
(b)
(c)
(d)
depth
correlation
skill
0
500
1000
1500
2000
2500
3000
3500
4000
4500
5000
0.0
0.1
0.2
0.3
0.4
0.5
0.6
0.7
0.8
0.9
1.0

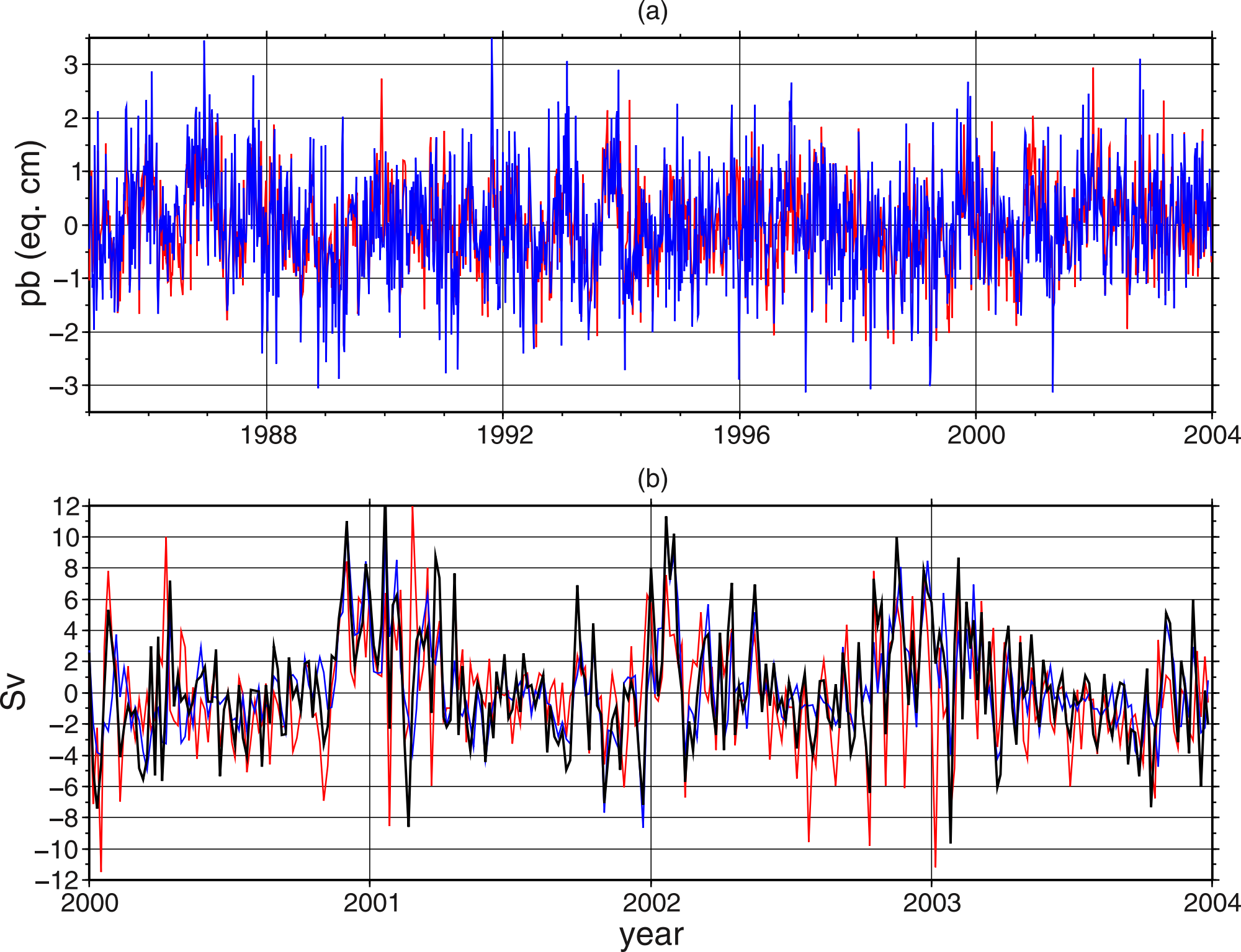
(a)
pb (eq. cm)
3
2
1
0
−1
−2
−3
1988
1992
1996
2000
2004
(b)
Sv
12
10
8
6
4
2
0
−2
−4
−6
−8
−10
−12
2000
2001
2002
2003
2004
year

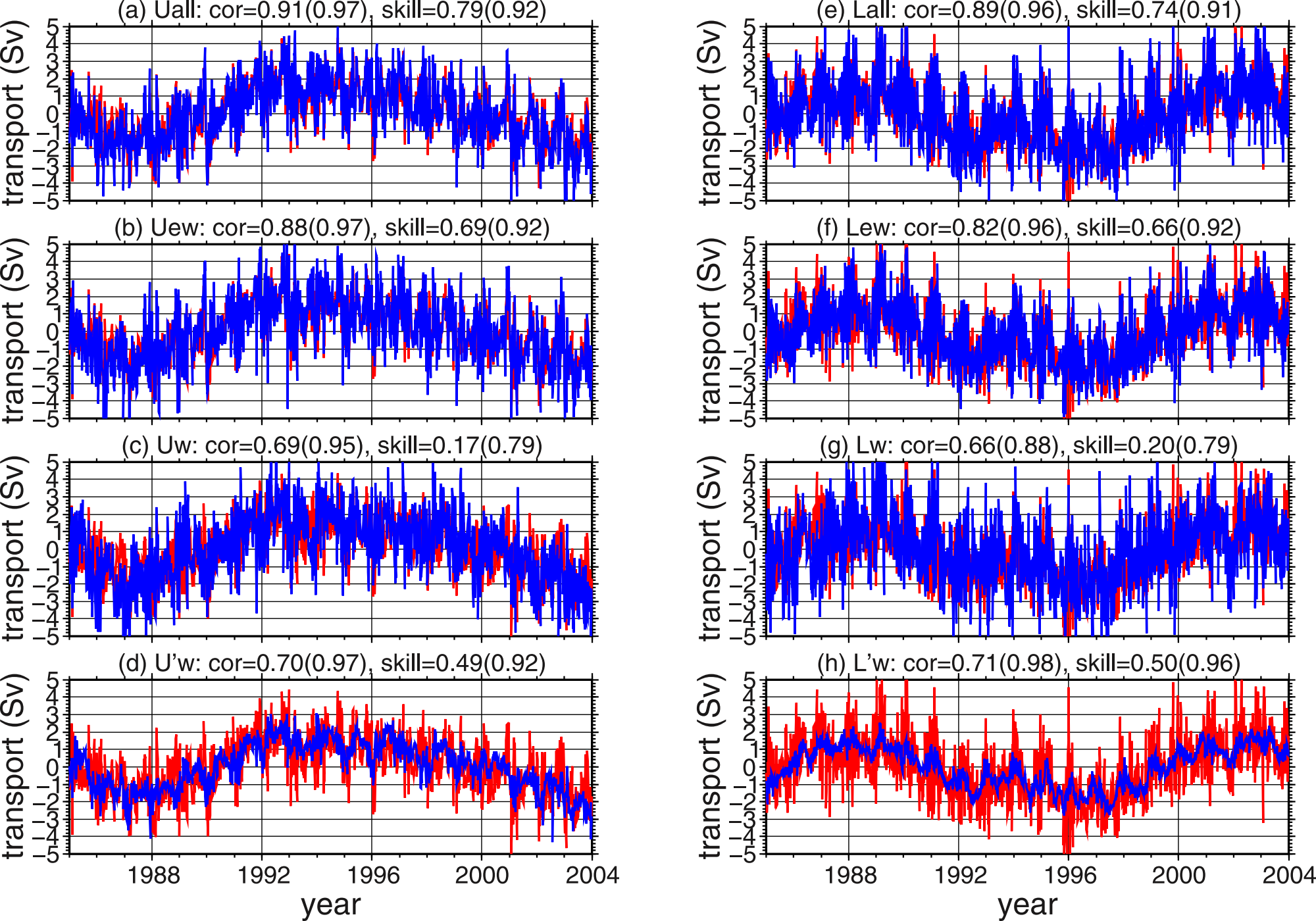
(a) Uall: cor=0.91(0.97), skill=0.79(0.92)
(b) Uew: cor=0.88(0.97), skill=0.69(0.92)
(c) Uw: cor=0.69(0.95), skill=0.17(0.79)
(d) U'w: cor=0.70(0.97), skill=0.49(0.92)
(e) Lall: cor=0.89(0.96), skill=0.74(0.91)
(f) Lew: cor=0.82(0.96), skill=0.66(0.92)
(g) Lw: cor=0.66(0.88), skill=0.20(0.79)
(h) L'w: cor=0.71(0.98), skill=0.50(0.96)
transport (Sv)
5
4
3
2
1
0
−1
−2
−3
−4
−5
1988
1992
1996
2000
2004
year

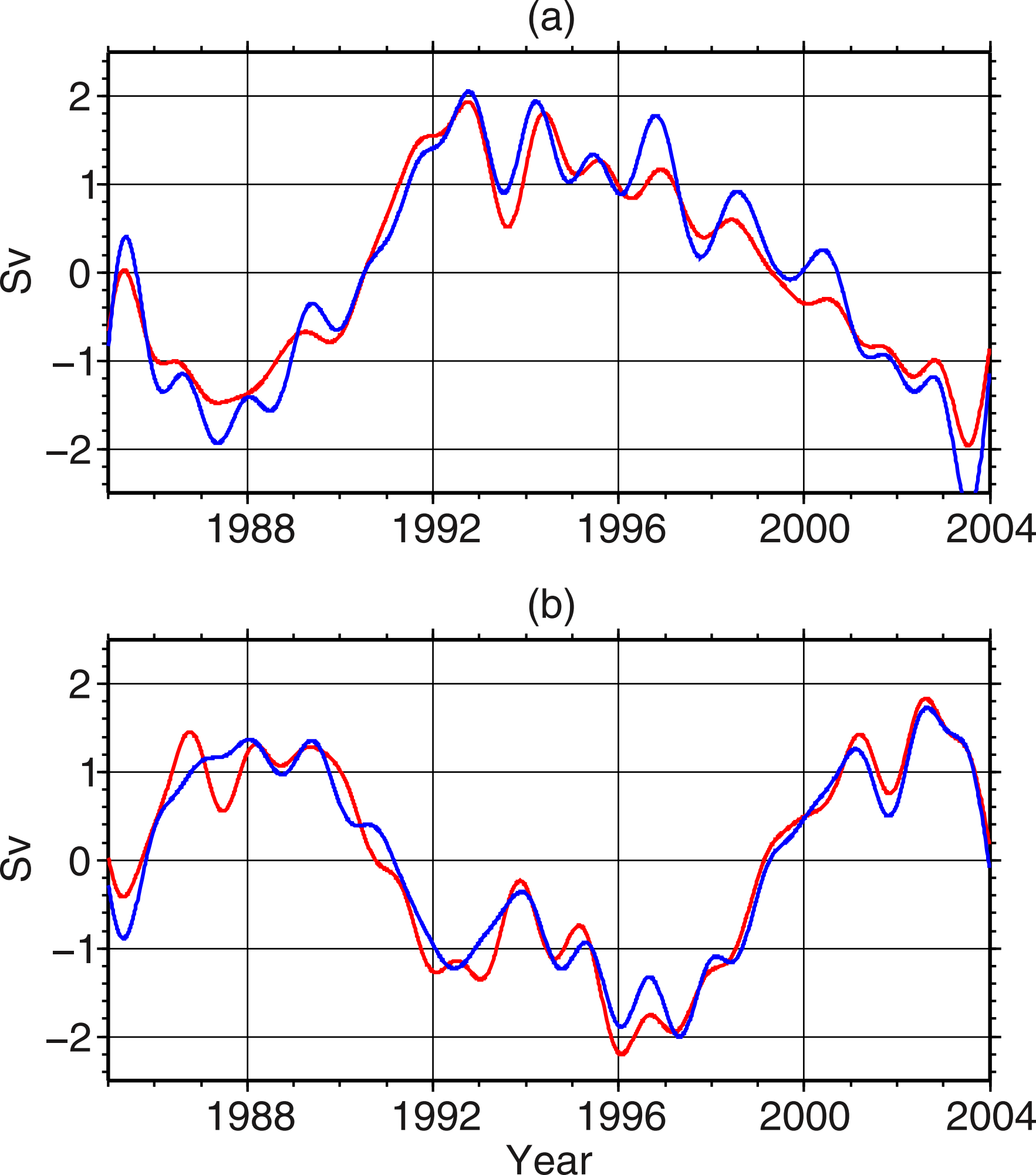
(a)
2
1
0
−1
−2
Sv
1988
1992
1996
2000
2004
(b)
2
1
0
−1
−2
Sv
1988
1992
1996
2000
2004
Year

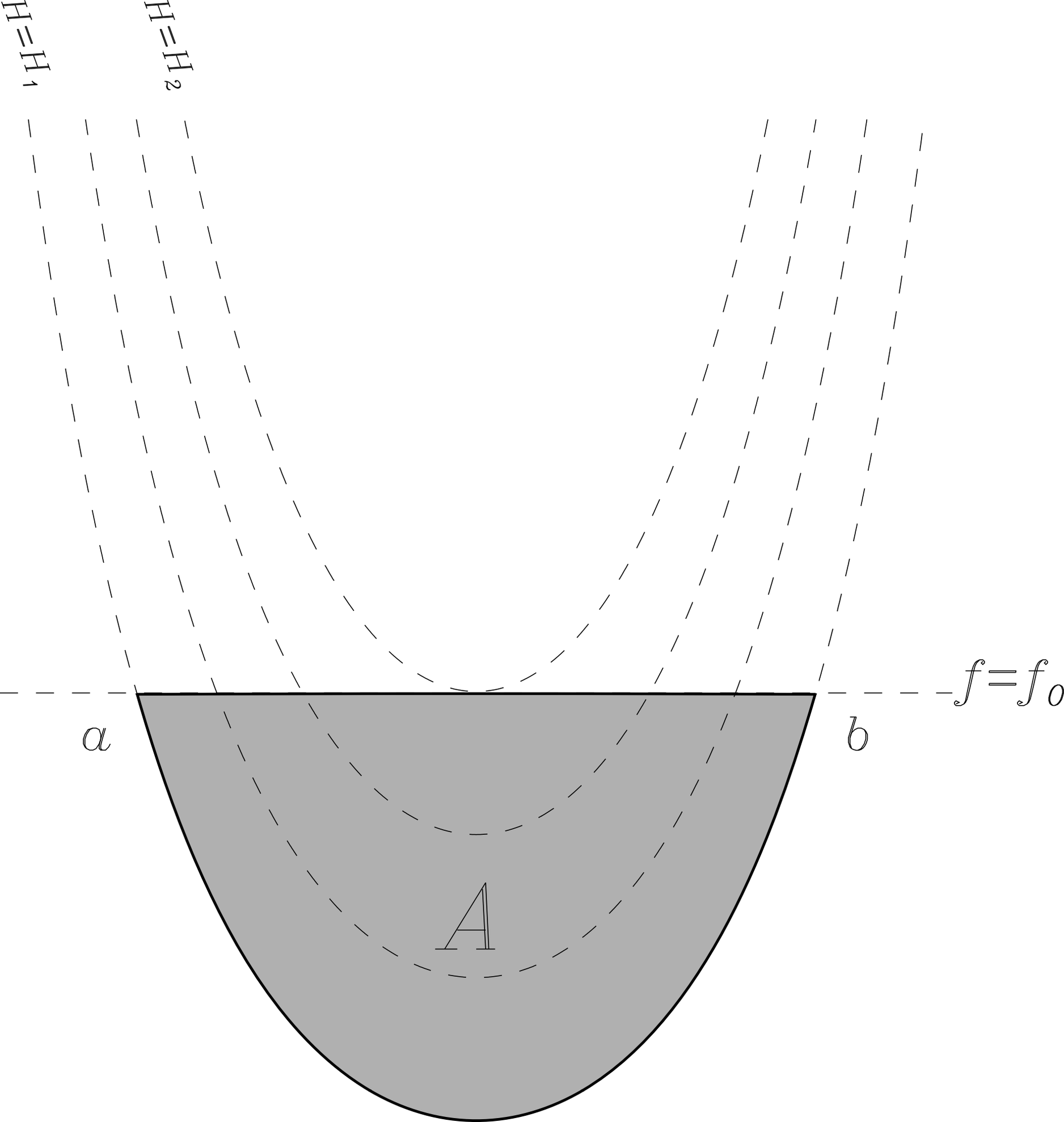
H=H1
H=H2
f=f0
a
b
A